Electronic Supplementary Material (ESI) for Physical Chemistry Chemical Physics.

ELECTRONIC SUPPLEMENTARY INFORMATION

Controlling Li^+ transport in ionic liquid electrolytes through salt content and anion asymmetry: A mechanistic understanding gained from molecular dynamics simulations

Alina Wettstein,[*,†] Diddo Diddens,[‡] and Andreas Heuer[*,‡,†]

[†]*Institut für physikalische Chemie, Westfälische Wilhelms-Universität Münster, Correnssstraße 28/30,*
D-48149 Münster, Germany

[‡]*Institut für Energie- und Klimaforschung, Ionics in Energy Storage, Helmholtz Institut Münster,,*
Forschungszentrum Jülich, Correnssstraße 46, 48149 Münster, Germany

E-mail: alina.wettstein@gmail.com; andheuer@wwu.de

A: Simulation protocol

All-atomistic molecular dynamics (MD) simulations of lithium salt-ionic liquid (IL) mixtures were performed using the software package GROMACS (version 2018.8).[1–4] The atomic interactions were parameterized according to well-established OPLS-AA[5]-derived CL&P force field developed by Canongia Lopes and Padua specifically for modeling ILs.[6–10]

Electronic polarization and charge transfer effects were accounted for in a mean field sense via rescaling the atomic point charges, which is the prevalent practice when relying on non-polarizable force fields to study ionic liquids,[11–20] because a more accurate treatment of the electronic polarizability by means of Drude oscillators[21] or induced point dipoles[22] comes at a great computational cost. Very recent studies on lithium salt-ionic liquid mixtures[17–20] and a variety of lithium salt containing electrolytes[14,15,23] have demonstrated successfully the ability of non-polarizable force fields, employing scaled partial charges, to capture and confirm experimental observations. In this work the the atomic point charges of all species were uniformly scaled down by a factor of 0.8.[11,17–20] We study structural and dynamical properties of the $\mathrm{Li}_x^+ - \mathrm{Pyr}_{14,(1-x)}^+ - \mathrm{TFSI}^-$ and $\mathrm{Li}_x^+ - \mathrm{Pyr}_{14,(1-x)}^+ - \mathrm{TFSAM}^-$ electrolytes in the same concentration range from $x = 0.0$ (neat IL) to $x = 0.7$ as experimentally reported in.[24]

The initial configurations were created with the PACKMOL software[25] which randomly distributed 1000 ion pairs, corresponding to the respective lithium salt to ionic liquid ratio, in a cubic box. The systems were first exposed to an energy minimization and then pre-equilibrated under NPT conditions for 40 ns at a high temperature of 500 K controlling pressure via a Berendsen barostat (relaxation time constant $\tau_P = 5.0\,\mathrm{ps}$, compressibility of 4.5×10^{-5} bar) coupled to a reference pressure of 1 bar and temperature via a velocity-rescale thermostat (relaxation time constant $\tau_T = 1.0\,\mathrm{ps}$).[26,27] Then the systems were cooled down to 400 K and equilibrated for another 100 ns. In the subsequent production run of 400 ns duration, that was used for data acquisition, pressure and temperature were coupled to an extended Parrinello-Rahman and Nosé-Hoover ensemble using the same relaxation time constants as before.[28–31] The equations of motion were solved via the leap-frog algorithm at a time step of 2 fs. The center of mass of the system was repositioned every simulation step. Furthermore, cutoffs for the long range electrostatic and the van der Waals interactions were both set to 1.4 nm and the linear constraint solver (LINCS) was employed to constrain the hydrogen bonds.[32,33] The simulation trajectories were analyzed with custom scripts supported by the Python library MDAnalysis.[34,35]

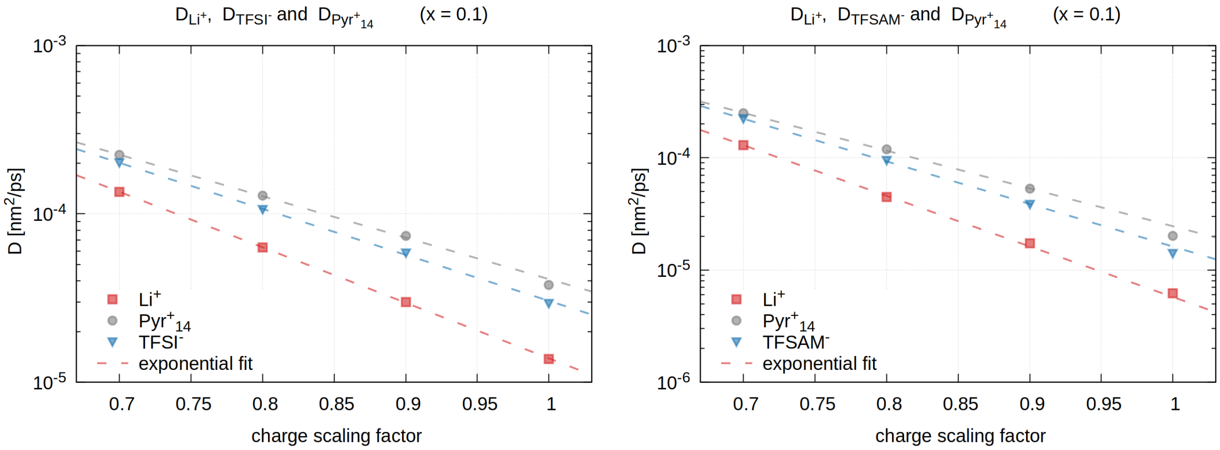

Figure S1: Self-diffusion coefficients D_i of all ionic species as a function of charge scaling factor γ for the TFSI$^-$ (left) and the TFSAM$^-$ system at a salt content of $\mathrm{x} = 0.1$. $\mathrm{D}_i(\gamma)$ is fitted (dashed lines) by an exponential function $f(\gamma) = a \cdot e^{b \cdot \gamma}$ ($b_{\mathrm{Li}^+} = -10.4$, $b_{\mathrm{Pyr}^+_{14}} = -7.6$ and $b_{\mathrm{TFSAM}^-} = -8.7$ for the TFSAM$^-$ system and $b_{\mathrm{Li}^+} = -7.6$, $b_{\mathrm{Pyr}^+_{14}} = -5.6$ and $b_{\mathrm{TFSI}^-} = -6.3$ for the TFSI$^-$ system), which can be interpreted as an Arrhenius-like behaviour. Weakened ionic interactions, *i.e.*, as expressed through lower γ values, might lower the activation barrier for diffusion which would thus result in faster ion dynamics. Comparison of D_i with preliminary results from polarizable FF simulations suggest a scaling factor $0.7 < \gamma < 0.8$. In order to avoid an over-scaling, we opted for $\gamma = 0.8$. The similar fitting values of b_i for the species in the respective mixture suggest that the relative dynamic trends are not distorted by the choice of γ.

B: Structural properties

The radial distribution functions $g_{\mathrm{Li^+\text{-}X}}$ are computed according to

$$g_{ab}(r) = \frac{V}{4\pi r^2 N_a N_b} \sum_{i=1}^{N_a} \sum_{j=1}^{N_b} \langle \delta \left(|\vec{\mathrm{r}}_i - \vec{\mathrm{r}}_j| - r \right) \rangle, \tag{S1}$$

where N_a/V and N_b/V denotes the average number density of species a and species b with V being the volume of the simulation box. The brackets $\langle .. \rangle$ indicate the ensemble average.

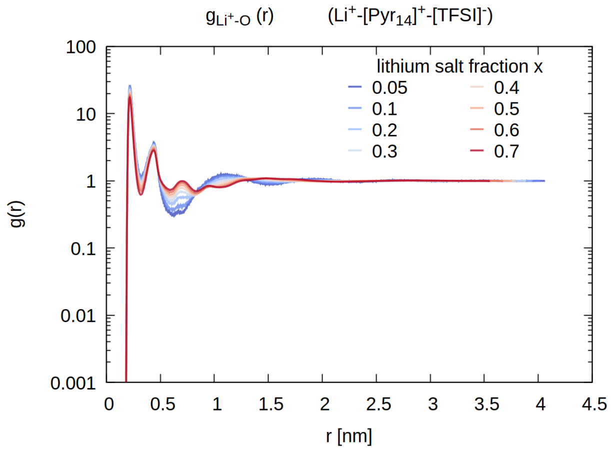
$g_{\mathrm{Li^+\text{-}O}}$ (r) (Li$^+$-[Pyr$_{14}$]$^+$-[TFSI]$^-$)

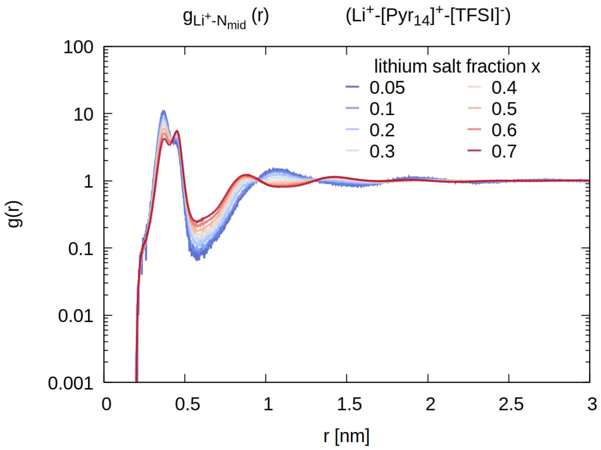
$g_{\mathrm{Li^+\text{-}N_{mid}}}$ (r) (Li$^+$-[Pyr$_{14}$]$^+$-[TFSI]$^-$)

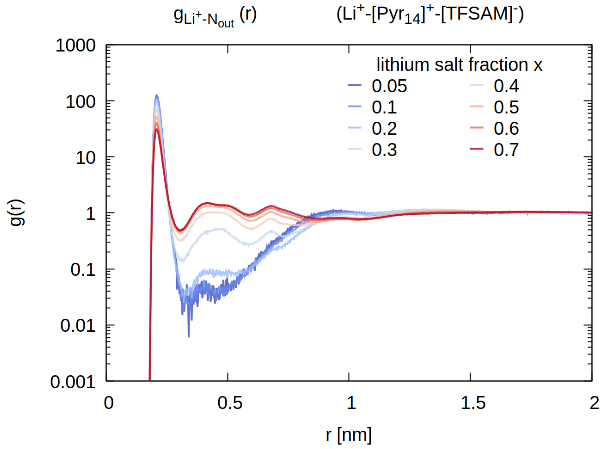
$g_{\mathrm{Li^+\text{-}N_{out}}}$ (r) (Li$^+$-[Pyr$_{14}$]$^+$-[TFSAM]$^-$)

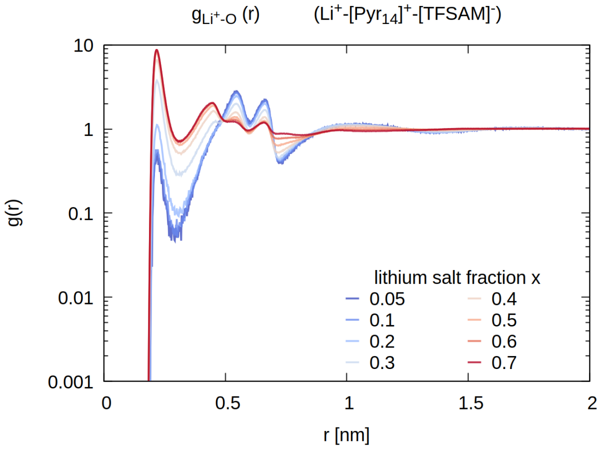
$g_{\mathrm{Li^+\text{-}O}}$ (r) (Li$^+$-[Pyr$_{14}$]$^+$-[TFSAM]$^-$)

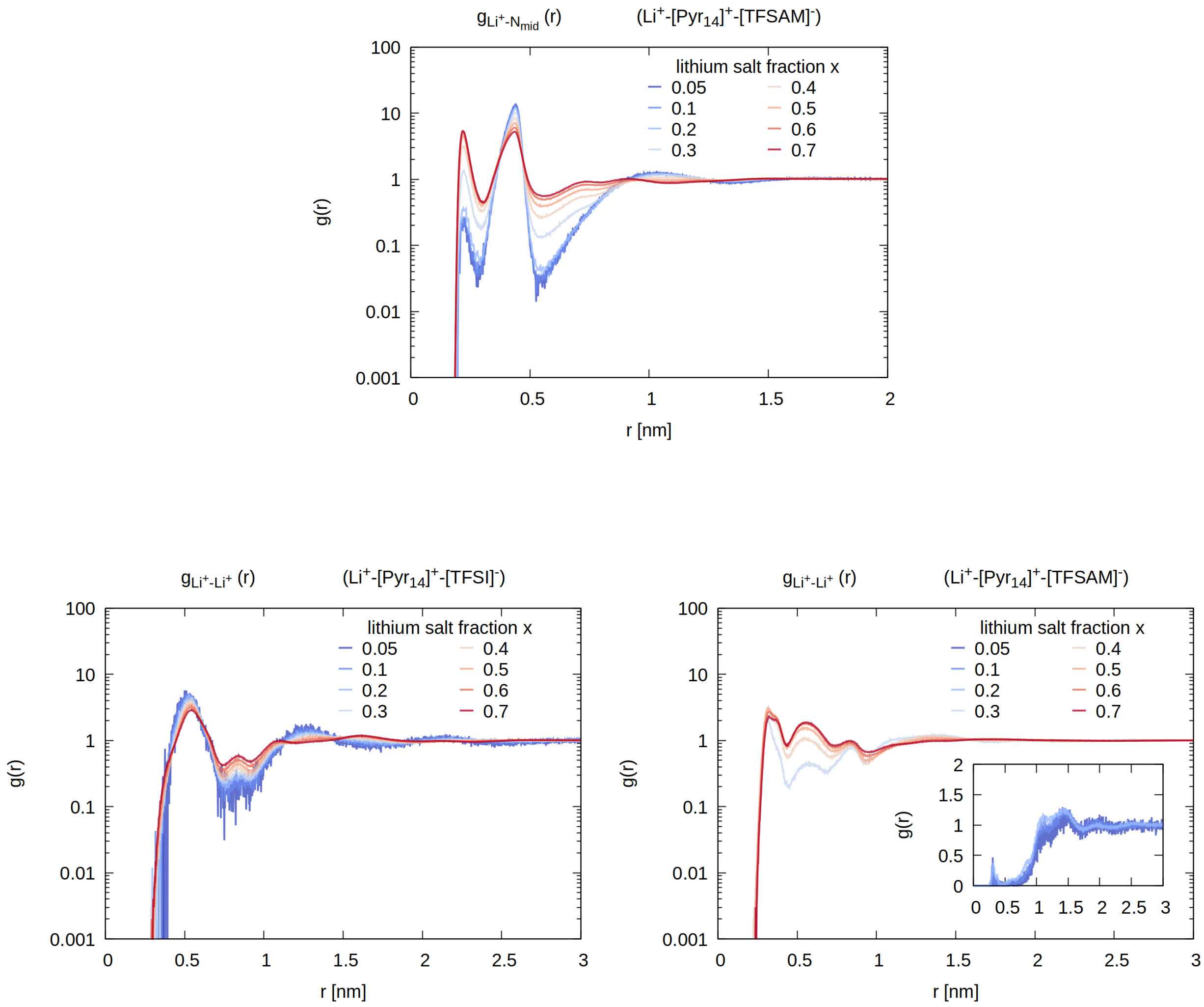

Figure S2: Overview of radial distribution functions $g_{Li^+-X}(r)$ between Li^+ ions and nitrogen / oxygen binding sites provided by $TFSI^-$ and $TFSAM^-$ as well as $g_{Li^+-Li^+}(r)$ in both electrolyte series on a log scale.

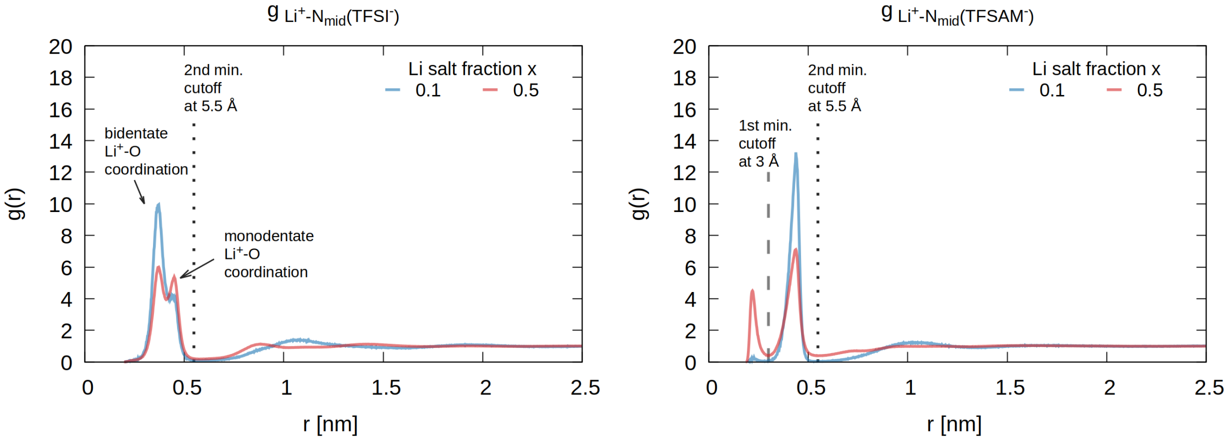

Figure S3: $g_{\mathrm{Li}^+-\mathrm{N}_{\mathrm{mid}}}$ for TFSI$^-$ and TFSAM$^-$ illustrate the choice of cutoff distance to determine current Li$^+$ – anion$^-$-binding, which is used for the computation of $\tau_{\mathrm{Li}^+-\mathrm{anion}^-}$.
The split peak structure of $g_{\mathrm{Li}^+-\mathrm{TFSI}^-(\mathrm{N}_{\mathrm{mid}})}$ results from the bidentate and monodentate coordination geometries. Using the position of the second minimum as a cutoff distance thus ensures that both motifs are included.
The double peak structure of $g_{\mathrm{Li}^+-\mathrm{TFSAM}^-(\mathrm{N}_{\mathrm{mid}})}$ can be explained in a similar way: At low salt contents, such as $\mathrm{x} = 0.1$, Li$^+$ binds almost exclusively with TFSAM$^-$ through $\mathrm{N}_{\mathrm{out}}$ (see Figure 1B in the main manuscript) which determines the peak position of $g_{\mathrm{Li}^+-\mathrm{TFSAM}^-(\mathrm{N}_{\mathrm{mid}})}$ at approximately 4 Å. In the highly concentrated mixtures, e.g., $\mathrm{x} = 0.5$, Li$^+$ is also coordinated by the less favorable $\mathrm{N}_{\mathrm{mid}}$ which is reflected in the emerging closer peak at approximately 3 Å. Thus, to decide if TFSAM$^-$ is part of the Li$^+$-solvation shell the second minimum position is used as the cutoff distance as well.

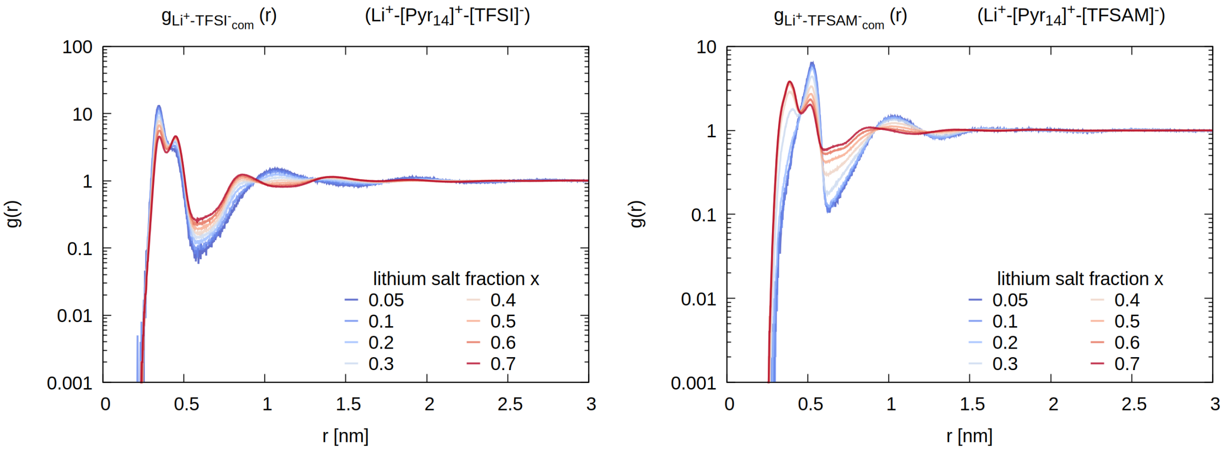

Figure S4: Overview of lithium - anion(com) radial distribution functions $\mathrm{g}_{\mathrm{Li}^+-\mathrm{anion}_{\mathrm{com}}}(\mathrm{r})$ on a log scale. The global minimum position is employed as the solvation shell size Ls in analogy to the procedure introduced by Self et al.[14]

.

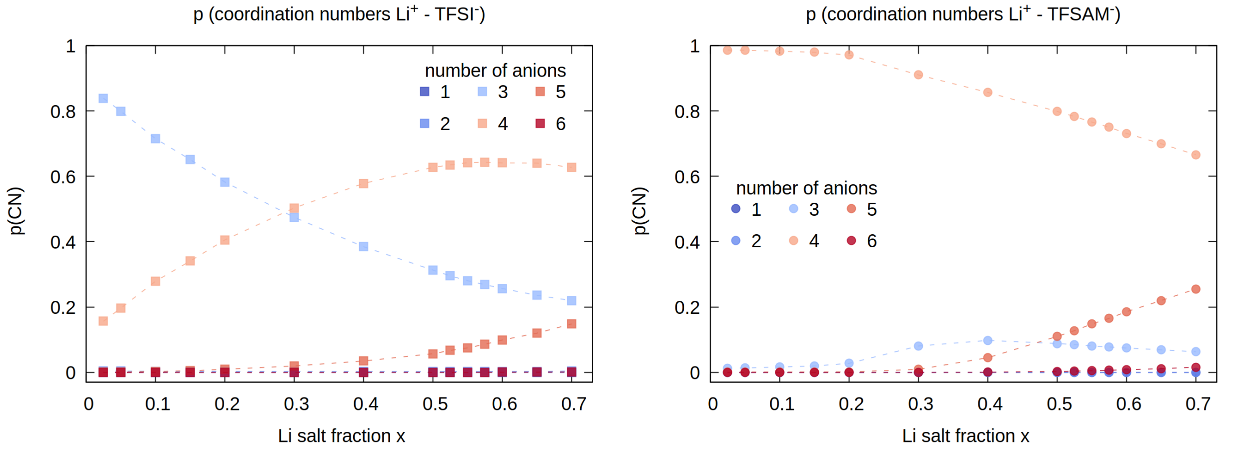

Figure S5: Probability distribution of Li^+-anion coordination numbers in the $TFSI^-$ (left) and $TFSAM^-$ (right) -based electrolytes as a function of lithium salt content x.

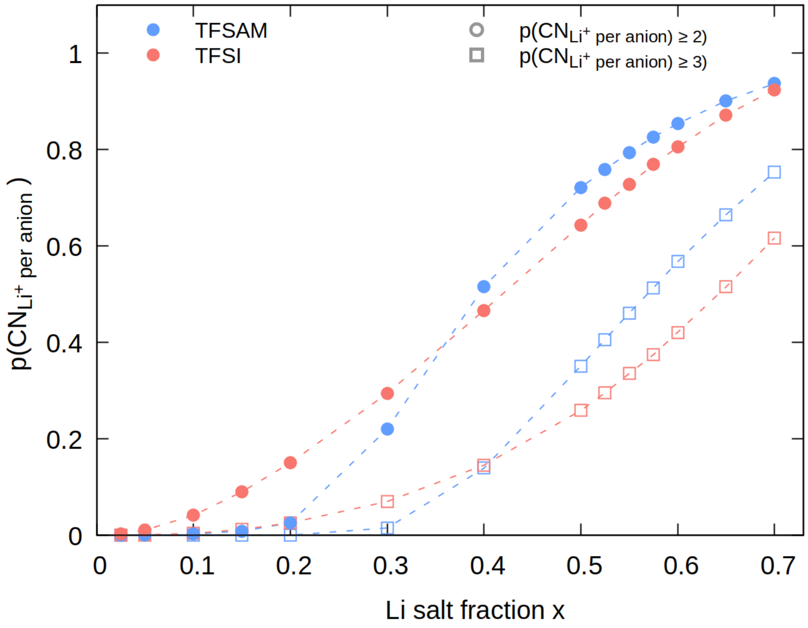

Figure S6: Probability distribution of lithium neighbors per $TFSI^-$/$TFSAM^-$ $p(CN_{Li^+ \text{per anion}})$ as a function of lithium salt content x.

C: Mean squared displacements

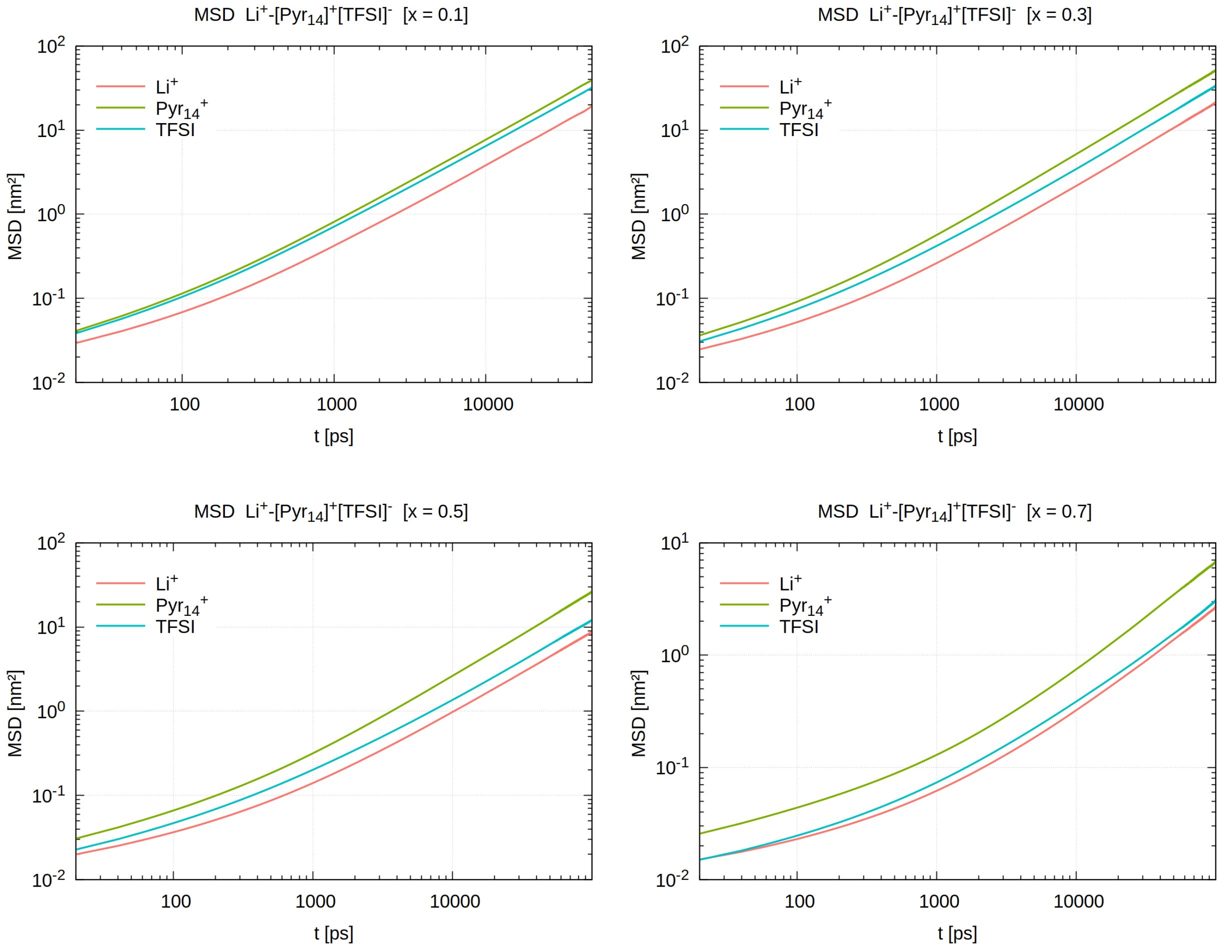

Figure S7: Example mean squared displacements of $\mathrm{Li}^+, \mathrm{Pyr}_{14}^+$ and TFSI^- as a function of time for lithium salt contents x=0.1 and x=0.3 (top) as well as x=0.5 and x=0.7 (bottom).

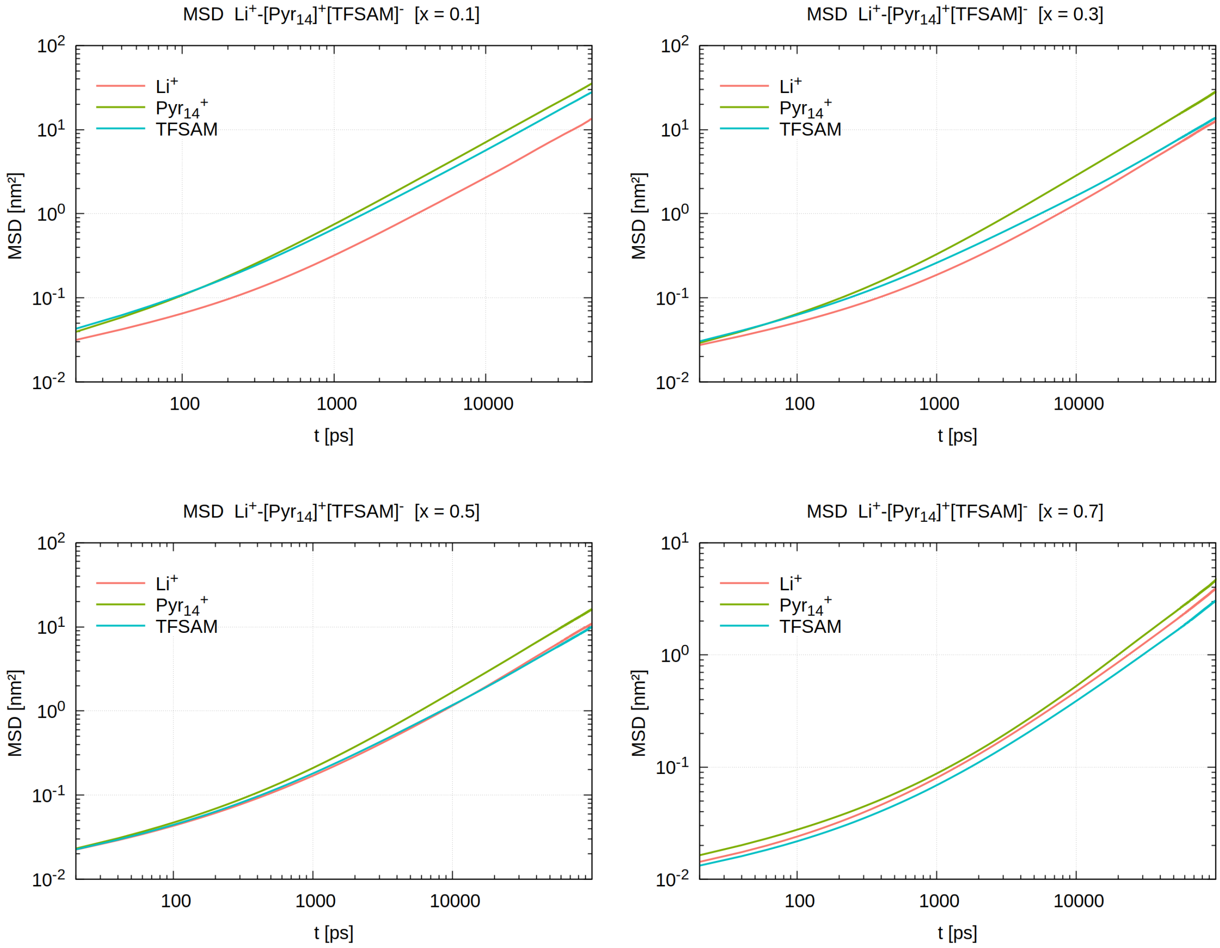

Figure S8: Example mean squared displacements of Li^+, Pyr_{14}^+ and TFSAM^- as a function of time for lithium salt contents x=0.1 and x=0.3 (top) as well as x=0.5 and x=0.7 (bottom).

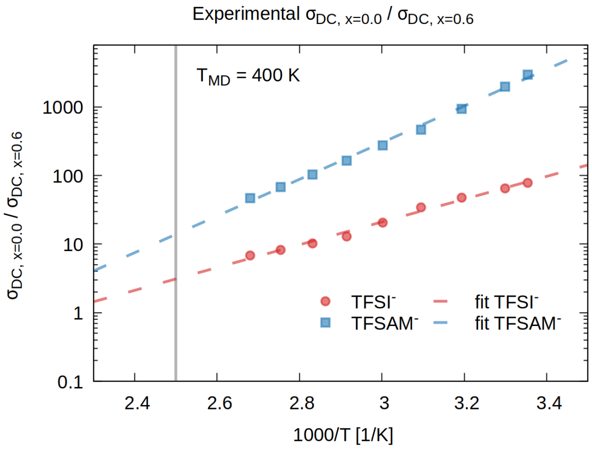

Figure S9: Investigation of the temperature dependence of the concentration-induced deceleration of transport properties on the basis of experimentally measured DC conductivities $\sigma_{\rm DC}$ taken from the work of Nüernberg et al.[24] $\sigma_{\rm DC}(\mathrm{x}=0.0)/\sigma_{\rm DC}(\mathrm{x}=0.6)(\mathrm{T})$ is compared for the TFSI$^-$ systems (red) and the TFSAM$^-$ analogue (blue). The temperature dependence can be well-described by an Arrhenius relation as demonstrated by the exponential fitting to $f(T) = a \cdot e^{b \cdot \frac{1000}{T}}$ (dashed lines). Reprinted (adapted) with permission from P. Nürnberg, E. I. Lozinskaya, A. S. Shaplov and M. Schönhoff, *The Journal of Physical Chemistry B*, 2020, **124**, 861–870. Copyright 2020 American Chemical Society.

D: Mean residence times

The mean residence times shown in Figure 5A and B in the main manuscript are calculated in four steps: Firstly, we define a neighbour function $H_{l\,x}(t)$ which counts 1 if a Li$^+$ particle l and a particle x belonging to species X are closer than a specific cutoff distance L_cut and 0 if they are further apart:

$$H_{l\,x}(t) \qquad = \qquad \begin{cases} 1, & \text{if particle}\, x \,\text{is inside l's solvation shell at time}\, t \\ 0, & \text{otherwise.} \end{cases} \tag{S2}$$

If not mentioned otherwise, the first minimum position of the radial distribution function $g_{\text{Li}^+ - X}(r)$ is employed as the cutoff distance L_cut to determine present Li$^+ - X$ binding. Please see $g_{\text{Li}^+ - \text{N}_\text{mid}}(r)$ for both TFSI$^-$- and TFSAM$^-$-containing mixtures in Figure S3 for an illustration of L_cut.

In the second step, we compute the autocorrelation function (ACF) of $H_{l\,x}(t)$ which thus measures the probability that a specific Li$^+ - X$ pair, which was formed at t_0, is a pair after time t has passed:[14,36–38]

$$p_{\text{Li}^+ - X}(t) = \frac{\langle\, H_{l\,x}(t_0) \;\cdot\; H_{l\,x}(t_0 + t)\,\rangle}{\langle\, H_{l\,x}(t_0) \;\cdot\; H_{l\,x}(t_0)\,\rangle}. \tag{S3}$$

The brackets $\langle .. \rangle$ denote the ensemble average over all pairs Li$^+ - X$ and time origins t_0. Empirically, these relaxation processes can be well-described by stretched exponential functions such as the Kohlrausch-Williams-Watts (KWW) function.[36,38–40] In a third step, we thus fit the probability distribution $p_{\text{Li}^+ - X}(t)$ to a stretched exponential $f(t)$:

$$f(t) = \exp\left(-(t/\tau')^\beta\right), \tag{S4}$$

where β and τ' are the fitting parameters. In the last step, the mean residence time $\tau_{\text{Li}^+ - X}$

of Li^+ with species X is obtained from the integral of $f(t)$ according to

$$\tau_{\mathrm{Li}^+-X} = \int_0^\infty dt\, \exp\left(-(t/\tau')^\beta\right) = \frac{\tau'}{\beta}\Gamma\left(1/\beta\right), \tag{S5}$$

where Γ denotes the Gamma-function.

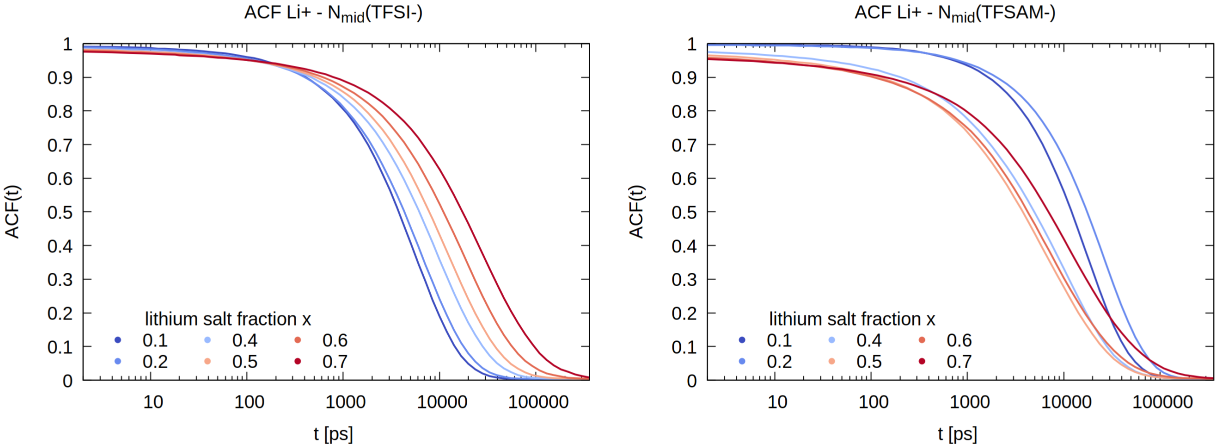

Figure S10: Exemplary overview of the concentration dependence of the autocorrelation functions of $\mathrm{Li}^+ - \mathrm{TFSI}^-$ and $\mathrm{Li}^+ - \mathrm{TFSAM}^-$ measured via $\mathrm{N}_{\mathrm{mid}}$ employing cutoffs of 5.5 Å .

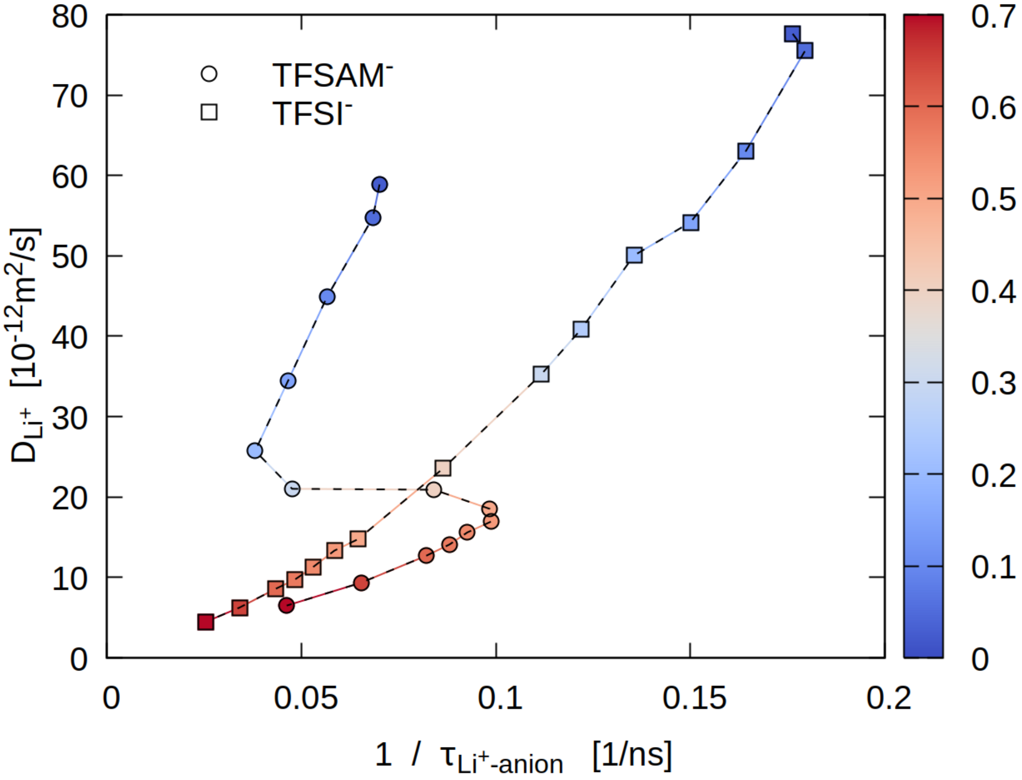

Figure S11: Relationship between Li^+ diffusivity D_{Li^+} (y-axis) and inverse Li^+-anion mean residence times $1/\tau_{\mathrm{Li}^+-\mathrm{anion}}$ (x-axis) as a function of salt concentration x (colour bar). The behaviour of the $TFSI^-$ systems is displayed by the square symbols, while the data points belonging to the $TFSAM^-$ systems are shown as circles.

E: Supporting information on the "self diffusion time" τ_{Ls}

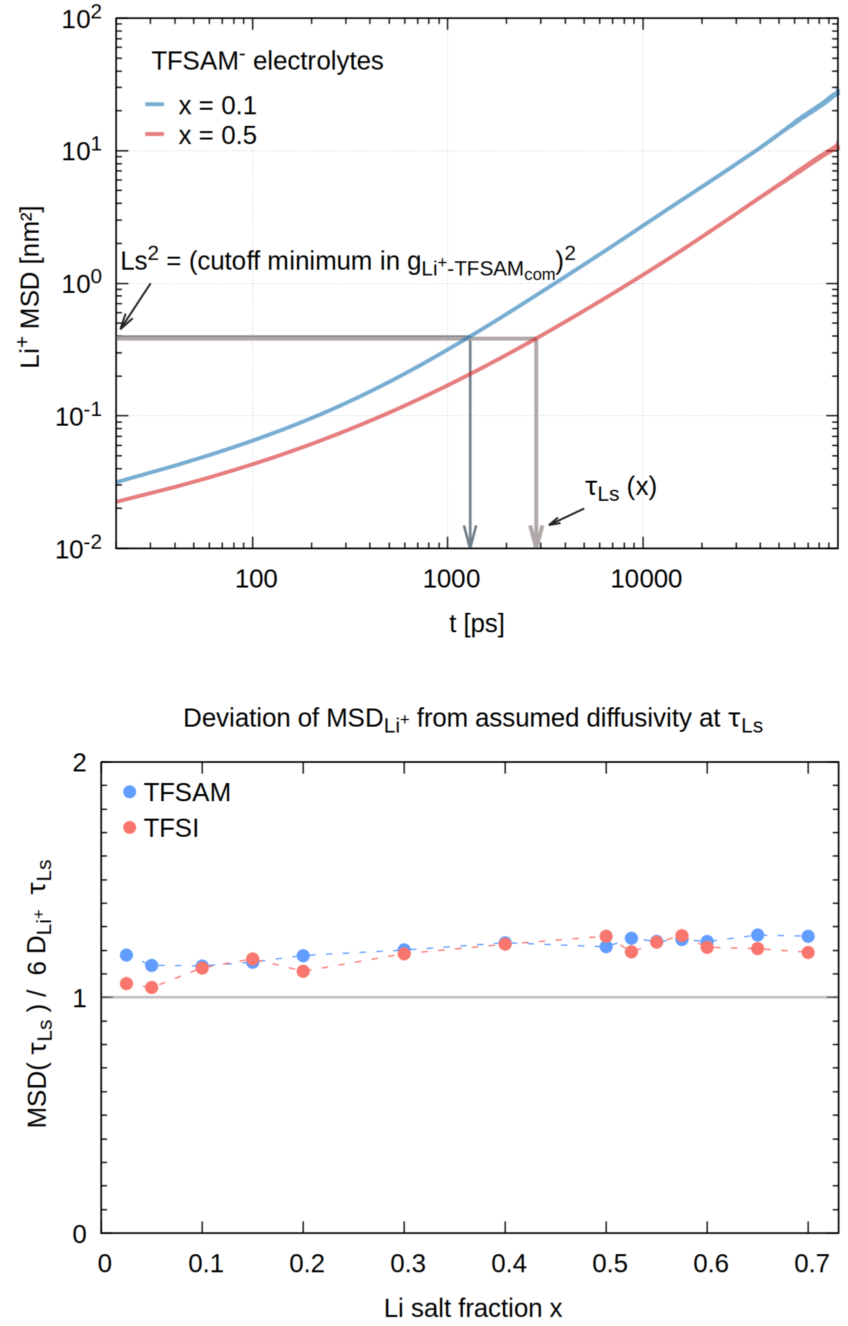

Figure S12: Top: Lithium mean squared displacement $\mathrm{MSD}_{\mathrm{Li}^+}$ as a function of time t for the $\mathrm{x} = 0.1$ and 0.5 TFSAM$^-$-based electrolytes. The arrow-flowchart depicts how the lithium "self-diffusion time" τ_{Ls} in a specific mixture is evaluated.

Bottom:Evaluating the deviation from purely diffusive lithium dynamics at critical time scale τ_{Ls}, i.e. $\mathrm{MSD}_{\mathrm{Li}^+}(\mathrm{t}) = 6\mathrm{D}_{\mathrm{Li}^+}\mathrm{t}$ at times τ_{Ls}.

F: $p(\Delta v_{\|})$ for various lag times and lithium subensembles

The panels in Figure S13 show the distributions $p(\Delta v_{\|})$ of TFSI$^-$ and TFSAM$^-$ relative distances in direction of the lithium displacement for salt concentrations $\mathrm{x} = 0.05$, 0.1, 0.2 and 0.5. The upper panels (a, b and c) display the histograms obtained for the anions whose designated lithium ions exhibit a squared displacement equal to the lithium mean squared displacement at the corresponding time t, i.e. $u^2 = 1 \cdot \langle u^2 \rangle$. The lower panels (d, e and f) measure $p(\Delta v_{\|})$ for the subensemble of lithium ions which achieved a squared displacement $u^2 = 3 \cdot \langle u^2 \rangle$.

In order to extent the statistical analysis of the subensembles to a larger data set, we introduce a tolerance interval $\{u_\mathrm{l}^2 \leq u^2 \leq u_\mathrm{r}^2\}$, whose upper and lower boundaries u_l^2 and u_r^2 are set in such a way that the sampled average u^2 of the subensemble corresponds to the target $k \cdot \langle u^2 \rangle$ (see Table S1). Because the lithium ions' individual squared displacements are normally distributed the threshold boundaries cannot be chosen symmetrically.

To characterize the peak positions and widths, we proceed according to the following protocol:

1. $\Delta v_{\|}$ is measured according to Equation 5 in the main manuscript and discretized employing a bin width of 0.1 Å and normalized. For reasons of visual appearance the histograms shown in the panels employ a bin width of 0.5 Å.

2. The obtained histogram $p(\Delta v_{\|})$ is empirically fitted by a Gaussian function
   $g(x) = \tilde{a} \cdot \exp\left(\frac{(x - \tilde{\mu})^2}{2\tilde{\sigma}^2}\right)$
   with the amplitude $\tilde{a}$, the expected value $\tilde{\mu}$ and variance $\tilde{\sigma}^2$.

3. Since anions naturally decouple from the lithium ion's dynamics upon detachment, it seems plausible that the distributions exhibit a skew towards negative $\Delta v_{\|}$ values. We find that an increasing amount of initial lithium-anion pairs has separated over time and is reflected in a growing tail of $p(\Delta v_{\|})$. To separate the peak features belonging to

the coupled lithium-anion dynamics from the overlapping distribution of dissociating dynamics, we restrict the left-hand side of the fit interval to $[-\tilde{\sigma} + \tilde{\mu}, \infty)$. The peak is refitted by a Gaussian function (red) $g(x) = a \cdot \exp\left(\frac{(x-\mu)^2}{2\sigma^2}\right)$ with the amplitude a, the expected value μ and variance σ^2.

4. Due to the significantly shorter mean residence times $\tau_{\mathrm{Li^+-TFSI^-}}$ compared to $\tau_{\mathrm{Li^+-TFSAM^-}}$ as discussed in the main manuscript, $p(\Delta v_{\|})$ is more disintegrated for TFSI$^-$ at the longest analysed lag time of $t = 10\,\mathrm{ns}$. Since the fit protocol step (3) fails to expose the peak originating from yet retained coupled dynamics, we fitted the peak manually (dashed orange).

Table S1: Overview of numerically determined lower boundaries u_{l}^2 for a given distance scaling factor k and upper tolerance thresholds u_{r}^2 of either 1.3 or 1.5, *i.e.*, 30 or 50 percent tolerance for lithium ions covering a squared distance larger than the target u^2.

k	u^2	u_{l}^2	u_{r}^2
1	$1 \cdot \langle u^2 \rangle$	$u^2 \,/\, 1.33$	$u^2 \cdot 1.3$
3	$3 \cdot \langle u^2 \rangle$	$u^2 \,/\, 1.22$	$u^2 \cdot 1.3$
1	$1 \cdot \langle u^2 \rangle$	$u^2 \,/\, 1.58$	$u^2 \cdot 1.5$
3	$3 \cdot \langle u^2 \rangle$	$u^2 \,/\, 1.31$	$u^2 \cdot 1.5$

At the very bottom of Figure S13, $p(\Delta v_{\|})$ is additionally shown for the explicit lithium binding sites provided by the respective anion, *i.e.*, TFSI$^-$(O) and TFSAM$^-$(N$_{\mathrm{out}}$) at x = 0.1.

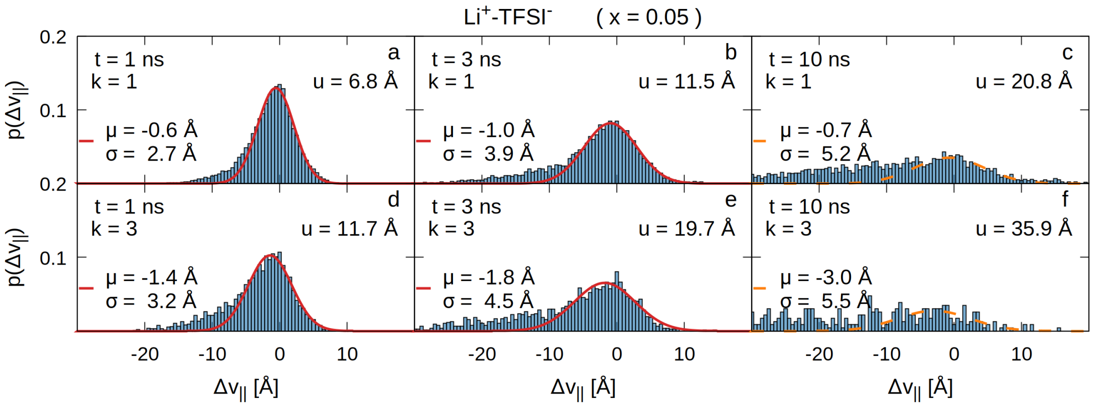
Li$^+$-TFSI$^-$ (x = 0.05)
p(Δv$_{||}$)
0.2
0.1
a
t = 1 ns
k = 1
u = 6.8 Å
μ = -0.6 Å
σ = 2.7 Å
b
t = 3 ns
k = 1
u = 11.5 Å
μ = -1.0 Å
σ = 3.9 Å
c
t = 10 ns
k = 1
u = 20.8 Å
μ = -0.7 Å
σ = 5.2 Å
d
t = 1 ns
k = 3
u = 11.7 Å
μ = -1.4 Å
σ = 3.2 Å
e
t = 3 ns
k = 3
u = 19.7 Å
μ = -1.8 Å
σ = 4.5 Å
f
t = 10 ns
k = 3
u = 35.9 Å
μ = -3.0 Å
σ = 5.5 Å
-20
-10
0
10
Δv$_{||}$ [Å]

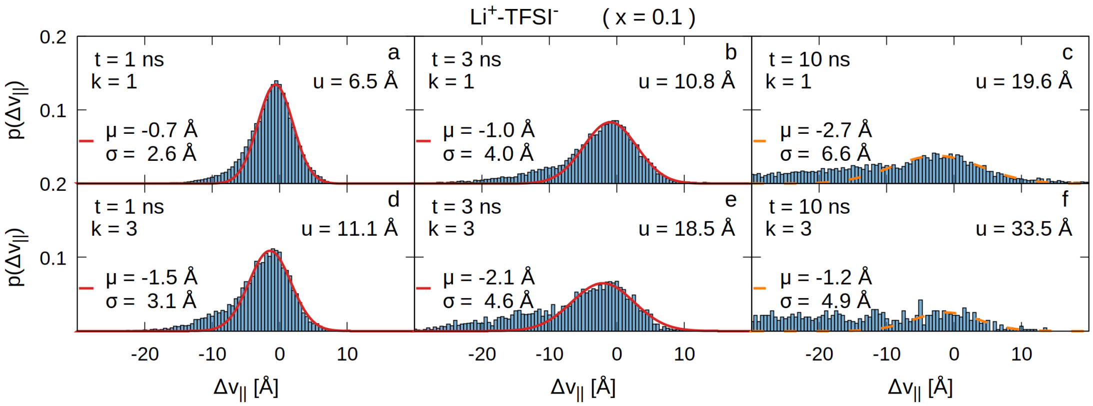
Li$^+$-TFSI$^-$ (x = 0.1)
p(Δv$_{||}$)
0.2
0.1
a
t = 1 ns
k = 1
u = 6.5 Å
μ = -0.7 Å
σ = 2.6 Å
b
t = 3 ns
k = 1
u = 10.8 Å
μ = -1.0 Å
σ = 4.0 Å
c
t = 10 ns
k = 1
u = 19.6 Å
μ = -2.7 Å
σ = 6.6 Å
d
t = 1 ns
k = 3
u = 11.1 Å
μ = -1.5 Å
σ = 3.1 Å
e
t = 3 ns
k = 3
u = 18.5 Å
μ = -2.1 Å
σ = 4.6 Å
f
t = 10 ns
k = 3
u = 33.5 Å
μ = -1.2 Å
σ = 4.9 Å
-20
-10
0
10
Δv$_{||}$ [Å]

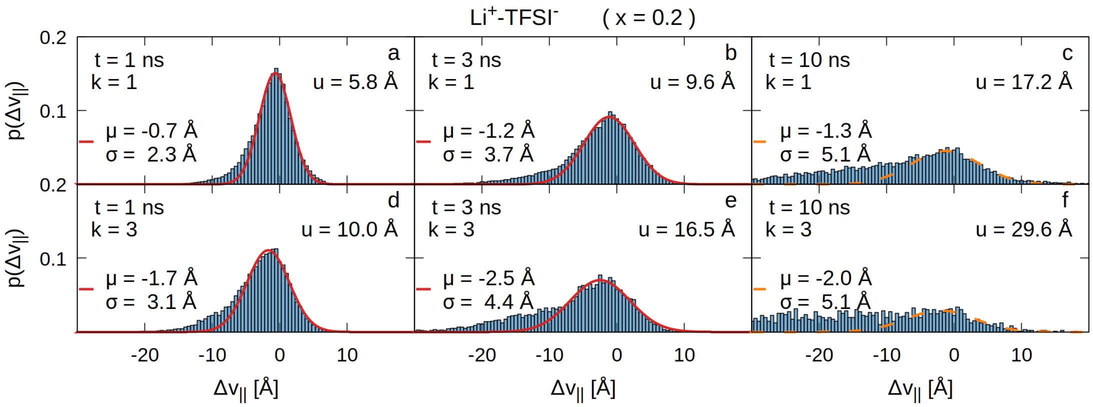
Li$^+$-TFSI$^-$ (x = 0.2)
p(Δv$_{||}$)
0.2
0.1
a
t = 1 ns
k = 1
u = 5.8 Å
μ = -0.7 Å
σ = 2.3 Å
b
t = 3 ns
k = 1
u = 9.6 Å
μ = -1.2 Å
σ = 3.7 Å
c
t = 10 ns
k = 1
u = 17.2 Å
μ = -1.3 Å
σ = 5.1 Å
d
t = 1 ns
k = 3
u = 10.0 Å
μ = -1.7 Å
σ = 3.1 Å
e
t = 3 ns
k = 3
u = 16.5 Å
μ = -2.5 Å
σ = 4.4 Å
f
t = 10 ns
k = 3
u = 29.6 Å
μ = -2.0 Å
σ = 5.1 Å
-20
-10
0
10
Δv$_{||}$ [Å]

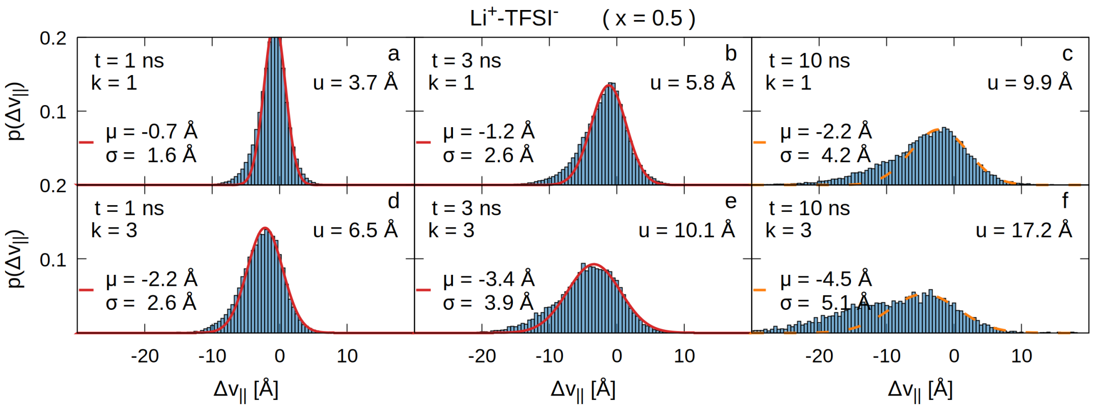
Li$^+$-TFSI$^-$ (x = 0.5)
p(Δv$_{||}$)
0.2
0.1
a
t = 1 ns
k = 1
u = 3.7 Å
μ = -0.7 Å
σ = 1.6 Å
b
t = 3 ns
k = 1
u = 5.8 Å
μ = -1.2 Å
σ = 2.6 Å
c
t = 10 ns
k = 1
u = 9.9 Å
μ = -2.2 Å
σ = 4.2 Å
d
t = 1 ns
k = 3
u = 6.5 Å
μ = -2.2 Å
σ = 2.6 Å
e
t = 3 ns
k = 3
u = 10.1 Å
μ = -3.4 Å
σ = 3.9 Å
f
t = 10 ns
k = 3
u = 17.2 Å
μ = -4.5 Å
σ = 5.1 Å
-20
-10
0
10
Δv$_{||}$ [Å]

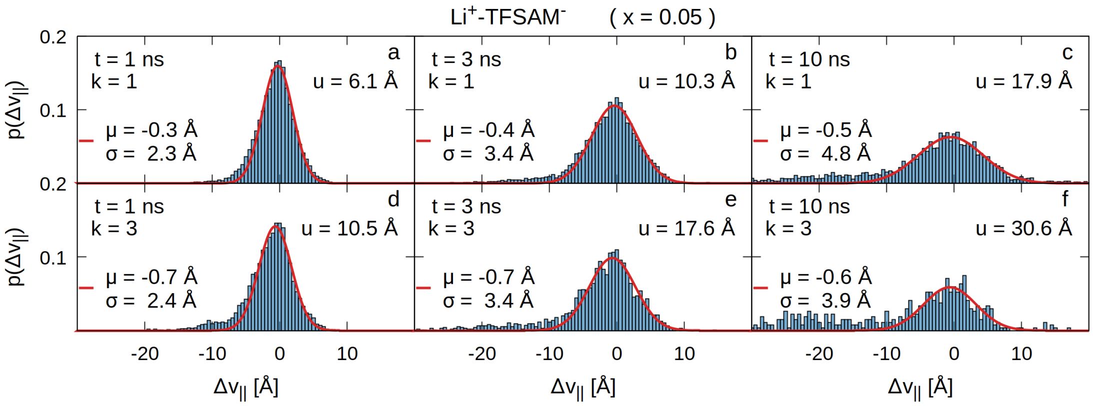
Li+-TFSAM- (x = 0.05)
p(Δv||)
0.2
0.1
a t = 1 ns k = 1 u = 6.1 Å μ = -0.3 Å σ = 2.3 Å
b t = 3 ns k = 1 u = 10.3 Å μ = -0.4 Å σ = 3.4 Å
c t = 10 ns k = 1 u = 17.9 Å μ = -0.5 Å σ = 4.8 Å
d t = 1 ns k = 3 u = 10.5 Å μ = -0.7 Å σ = 2.4 Å
e t = 3 ns k = 3 u = 17.6 Å μ = -0.7 Å σ = 3.4 Å
f t = 10 ns k = 3 u = 30.6 Å μ = -0.6 Å σ = 3.9 Å
-20 -10 0 10
Δv|| [Å]

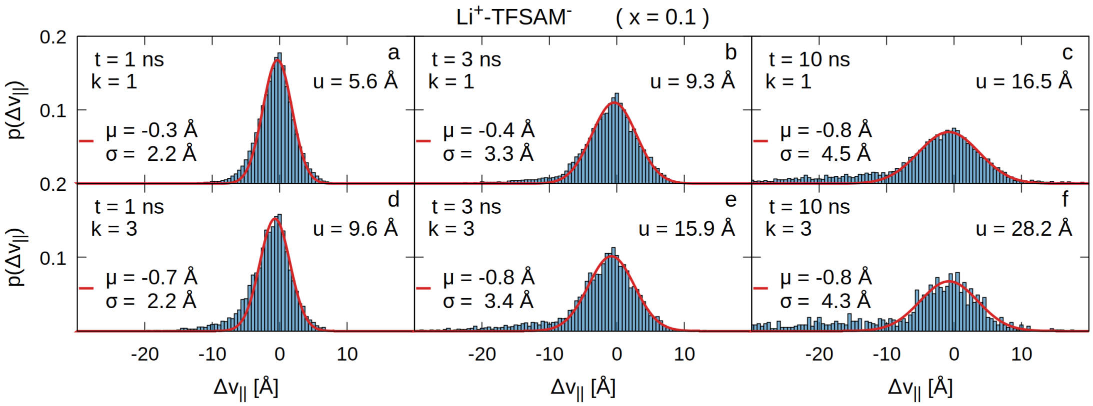
Li+-TFSAM- (x = 0.1)
p(Δv||)
0.2
0.1
a t = 1 ns k = 1 u = 5.6 Å μ = -0.3 Å σ = 2.2 Å
b t = 3 ns k = 1 u = 9.3 Å μ = -0.4 Å σ = 3.3 Å
c t = 10 ns k = 1 u = 16.5 Å μ = -0.8 Å σ = 4.5 Å
d t = 1 ns k = 3 u = 9.6 Å μ = -0.7 Å σ = 2.2 Å
e t = 3 ns k = 3 u = 15.9 Å μ = -0.8 Å σ = 3.4 Å
f t = 10 ns k = 3 u = 28.2 Å μ = -0.8 Å σ = 4.3 Å
-20 -10 0 10
Δv|| [Å]

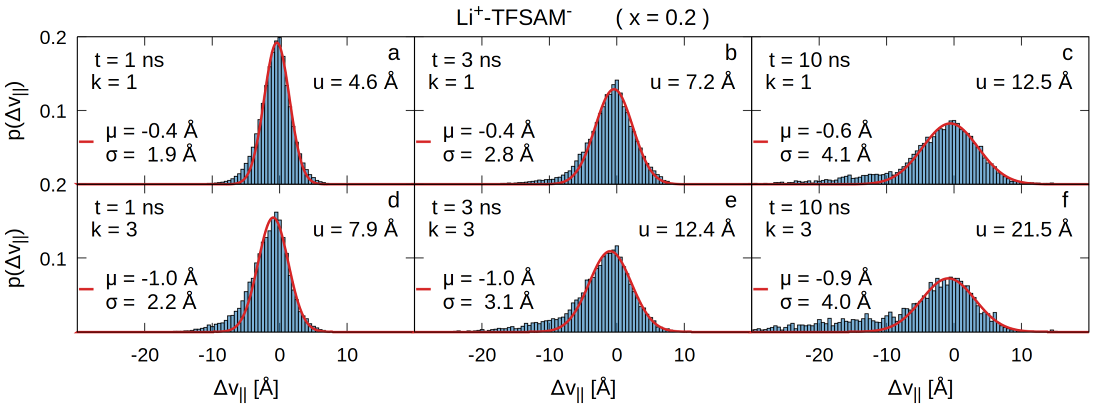
Li+-TFSAM- (x = 0.2)
p(Δv||)
0.2
0.1
a t = 1 ns k = 1 u = 4.6 Å μ = -0.4 Å σ = 1.9 Å
b t = 3 ns k = 1 u = 7.2 Å μ = -0.4 Å σ = 2.8 Å
c t = 10 ns k = 1 u = 12.5 Å μ = -0.6 Å σ = 4.1 Å
d t = 1 ns k = 3 u = 7.9 Å μ = -1.0 Å σ = 2.2 Å
e t = 3 ns k = 3 u = 12.4 Å μ = -1.0 Å σ = 3.1 Å
f t = 10 ns k = 3 u = 21.5 Å μ = -0.9 Å σ = 4.0 Å
-20 -10 0 10
Δv|| [Å]

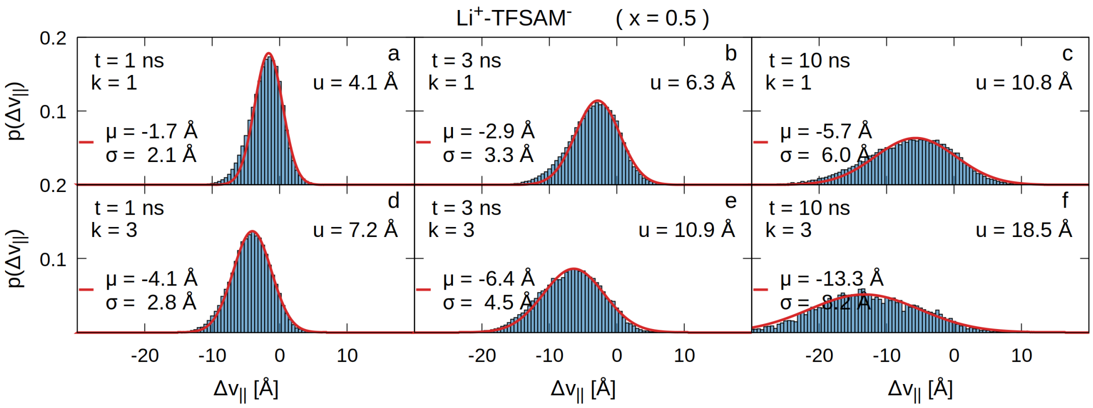
Li+-TFSAM- (x = 0.5)
p(Δv||)
0.2
0.1
a t = 1 ns k = 1 u = 4.1 Å μ = -1.7 Å σ = 2.1 Å
b t = 3 ns k = 1 u = 6.3 Å μ = -2.9 Å σ = 3.3 Å
c t = 10 ns k = 1 u = 10.8 Å μ = -5.7 Å σ = 6.0 Å
d t = 1 ns k = 3 u = 7.2 Å μ = -4.1 Å σ = 2.8 Å
e t = 3 ns k = 3 u = 10.9 Å μ = -6.4 Å σ = 4.5 Å
f t = 10 ns k = 3 u = 18.5 Å μ = -13.3 Å σ = 9.2 Å
-20 -10 0 10
Δv|| [Å]

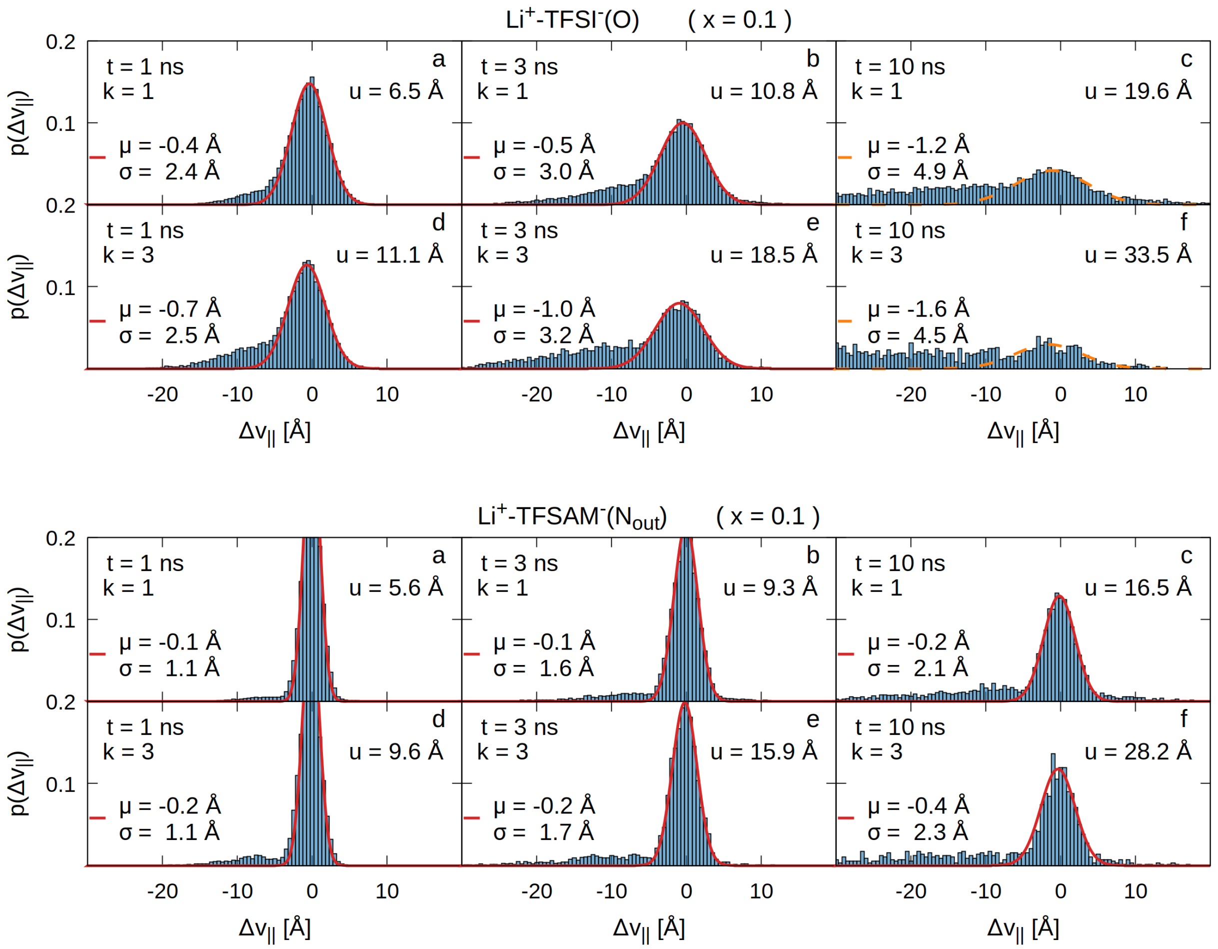

Figure S13: Distributions $p(\Delta v_{\|})$ of TFSI$^-$ and TFSAM$^-$ for the subensembles of $u^2 = k \cdot \langle u^2 \rangle$ with $k = 1$ (a,b and c) and 3 (d, e and f) for various lag times t and salt concentrations x using an upper threshold tolerance $u_\mathrm{r}^2 = 1.5 \cdot k \cdot \langle u^2 \rangle$.

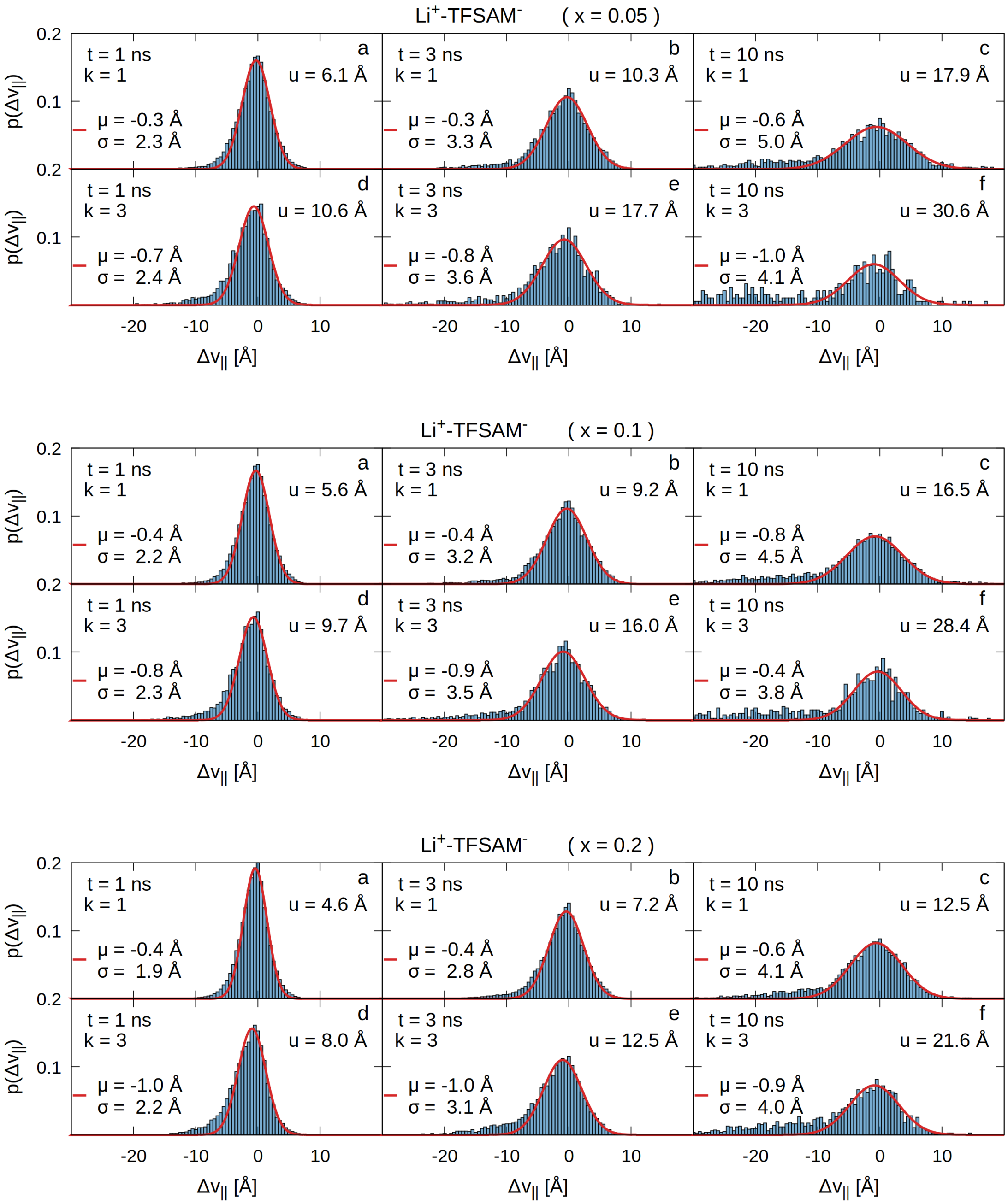

Figure S14: Distributions $p(\Delta v_{\|})$ of TFSAM$^-$ at a salt concentration x = 0.1 for the subensembles of $u^2 = k \cdot \langle u^2 \rangle$ with $k = 1$ (a, b and c) and 3 (d, e and f) using an upper threshold tolerance $u_{\mathrm{r}}^2 = 1.3 \cdot k \cdot \langle u^2 \rangle$.

G: Relationship of Gaussian peak parameters μ and σ^2 : A particle-spring-model approach

With the aim to understand why the Gaussian peak centers μ are not positioned at $\Delta v_{\parallel} = 0\,\text{Å}$ but increasingly shifted for a larger distance scaling factor k, we propose a simple thought experiment:

We idealize a lithium-anion-pair to behave like two particles that are coupled through a harmonic interaction, *i.e.*, connected by a spring. Since we analyse the anion dynamics in the reference frame of the lithium ion, the coupled dynamics reduce, firstly, to one spatial dimension and, secondly, can be conveniently expressed by the system's collective and relative displacements

$$\begin{aligned} X &= \frac{1}{2} \cdot \left(u + v_{\parallel}\right) \\ \Gamma &= \frac{1}{2} \cdot \left(u - v_{\parallel}\right) . \end{aligned} \tag{S6}$$

The collective coordinate X thus describes the diffusive motion of the coupled particles whereas the relative coordinate Γ measures the fluctuations of the particles' relative positions. Assuming a normal distribution for both, *i.e.*, $\mathcal{N}(\mu_X, \sigma_X^2)$ and $\mathcal{N}(\mu_\Gamma, \sigma_\Gamma^2)$, we can deduce the conditional probability distribution $P(v_{\parallel} - u|u)$ that we sampled in the histograms $p(\Delta v_{\parallel})$, starting with $P(v_{\parallel}|u) = P(u, v_{\parallel})/P(u)$:

$$\begin{aligned} P(u, v_{\parallel}) &\propto \mathcal{N}(\mu_X, \sigma_X^2) \cdot \mathcal{N}(\mu_\Gamma, \sigma_\Gamma^2) \\ &\propto \exp\left(-\frac{1}{2}\frac{(u + v_{\parallel})^2}{4\sigma_X^2}\right) \cdot \exp\left(-\frac{1}{2}\frac{(u - v_{\parallel})^2}{4\sigma_\Gamma^2}\right) \\ &\propto \exp\left(-\frac{1}{2} \cdot \frac{1}{4 \cdot AB/(A+B)^2}\left[v_{\parallel} - \underbrace{\frac{A-B}{A+B} \cdot u}_{\mu_{v_{\parallel}}}\right]^2\right) \cdot \exp(..) \quad \text{with} \quad A = \sigma_X^2 \quad B = \sigma_\Gamma^2 \end{aligned} \tag{S7}$$

Therefore, it holds for $\mu \doteq \mu_{\Delta v_\parallel}$:

$$\begin{aligned}\mu &= \mu_{v_\parallel} - u \\ &= \frac{\sigma_X^2 - \sigma_\Gamma^2}{\sigma_X^2 + \sigma_\Gamma^2} \cdot u - u \\ &= -2 \cdot \frac{\sigma_\Gamma^2}{\sigma_\Gamma^2 + \sigma_X^2} \cdot u\end{aligned} \tag{S8}$$

The variances σ_X^2 and σ_Γ^2 are related to the observables $\langle u^2 \rangle$ and $\sigma^2 \doteq \sigma_{\Delta v_\parallel}^2$ which are accessible through our analysis:

$$\sigma_u^2 = \langle u^2 \rangle - \underbrace{\langle u \rangle^2}_{0} \doteq \sigma_X^2 + \sigma_\Gamma^2 \qquad \wedge \qquad \sigma_\Gamma^2 = \frac{1}{4}\sigma^2. \tag{S9}$$

Consequently, we can rewrite Equation SS8:

$$\begin{aligned}\mu &= -\frac{u}{2} \cdot \frac{\sigma^2}{\langle u^2 \rangle} \\ &= -\frac{\sqrt{k}}{2} \cdot \frac{\sigma^2}{\sqrt{\langle u^2 \rangle}} \qquad \text{for} \qquad u^2 \;=\; k \cdot \langle u^2 \rangle.\end{aligned} \tag{S10}$$

The expression "masterscaling" in the main manuscript refers to a simple rearrangement of Equation SS10 :

$$1 = -2 \cdot \frac{\mu \sqrt{\langle u^2 \rangle}}{\sqrt{k}\sigma^2}. \tag{S11}$$

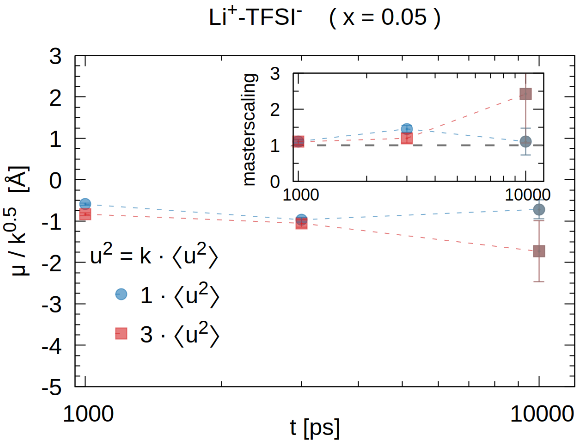
Li$^+$-TFSI$^-$ (x = 0.05)
μ / k$^{0.5}$ [Å]
t [ps]
1000
10000
3
2
1
0
-1
-2
-3
-4
-5
$u^2 = k \cdot \langle u^2 \rangle$
$1 \cdot \langle u^2 \rangle$
$3 \cdot \langle u^2 \rangle$
masterscaling
0
1
2
3
1000
10000

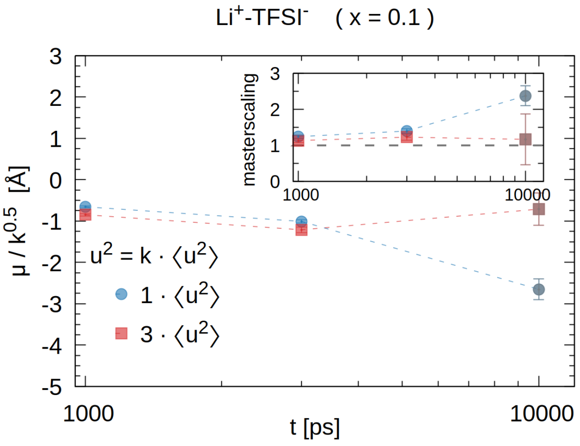
Li$^+$-TFSI$^-$ (x = 0.1)
μ / k$^{0.5}$ [Å]
t [ps]
1000
10000
3
2
1
0
-1
-2
-3
-4
-5
$u^2 = k \cdot \langle u^2 \rangle$
$1 \cdot \langle u^2 \rangle$
$3 \cdot \langle u^2 \rangle$
masterscaling
0
1
2
3
1000
10000

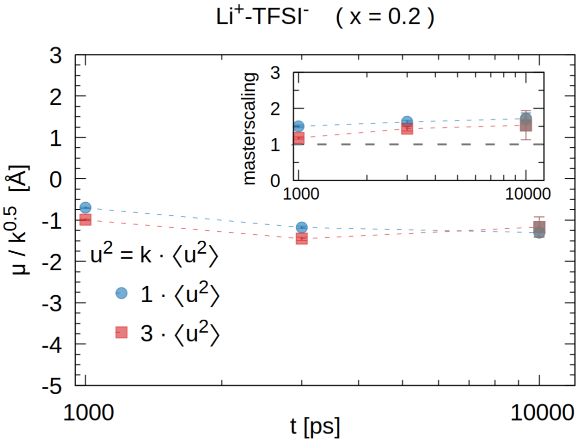
Li$^+$-TFSI$^-$ (x = 0.2)
μ / k$^{0.5}$ [Å]
t [ps]
1000
10000
3
2
1
0
-1
-2
-3
-4
-5
$u^2 = k \cdot \langle u^2 \rangle$
$1 \cdot \langle u^2 \rangle$
$3 \cdot \langle u^2 \rangle$
masterscaling
0
1
2
3
1000
10000

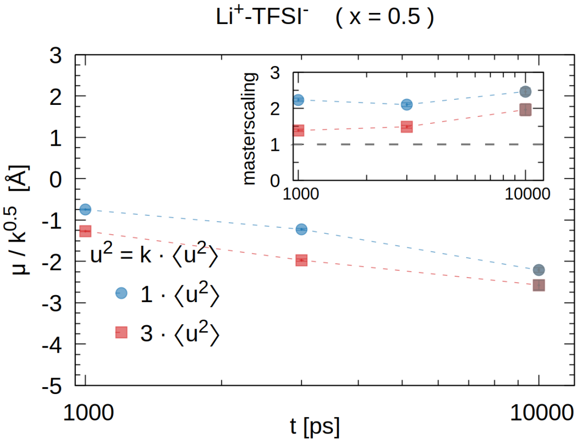
Li$^+$-TFSI$^-$ (x = 0.5)
μ / k$^{0.5}$ [Å]
t [ps]
1000
10000
3
2
1
0
-1
-2
-3
-4
-5
$u^2 = k \cdot \langle u^2 \rangle$
$1 \cdot \langle u^2 \rangle$
$3 \cdot \langle u^2 \rangle$
masterscaling
0
1
2
3
1000
10000

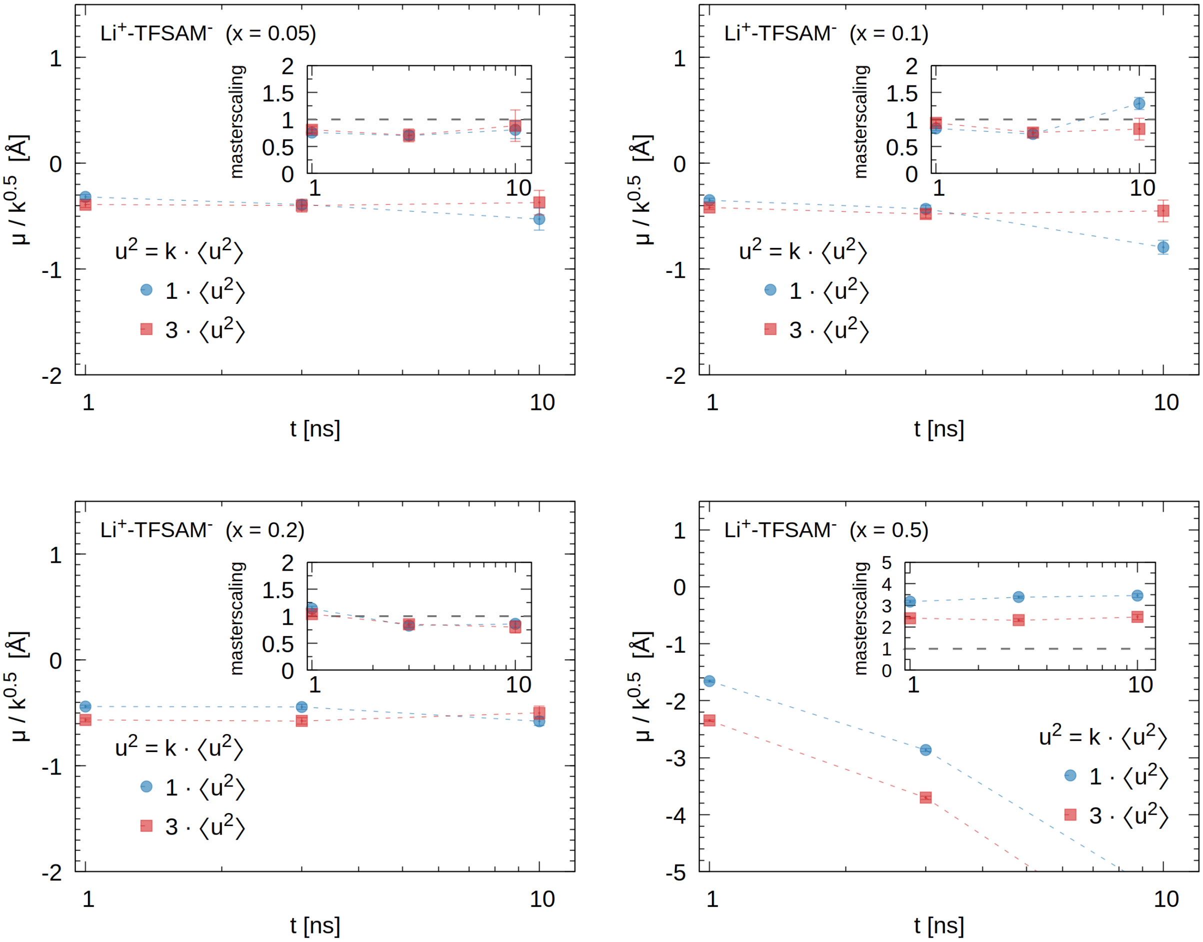

Figure S15: Gaussian peak positions $\mu(t)$ divided by the square root of the distance scaling factor k. Inset: Masterscaling of the Gaussian peak parameters μ and σ^2 to 1 according to Equation SS11. The data points relying on the manually performed Gaussian fits are highlighted in grey. The data points are based on measurements employing an upper threshold tolerance $u_{\mathrm{r}}^2 = 1.5 \cdot k \cdot \langle u^2 \rangle$.

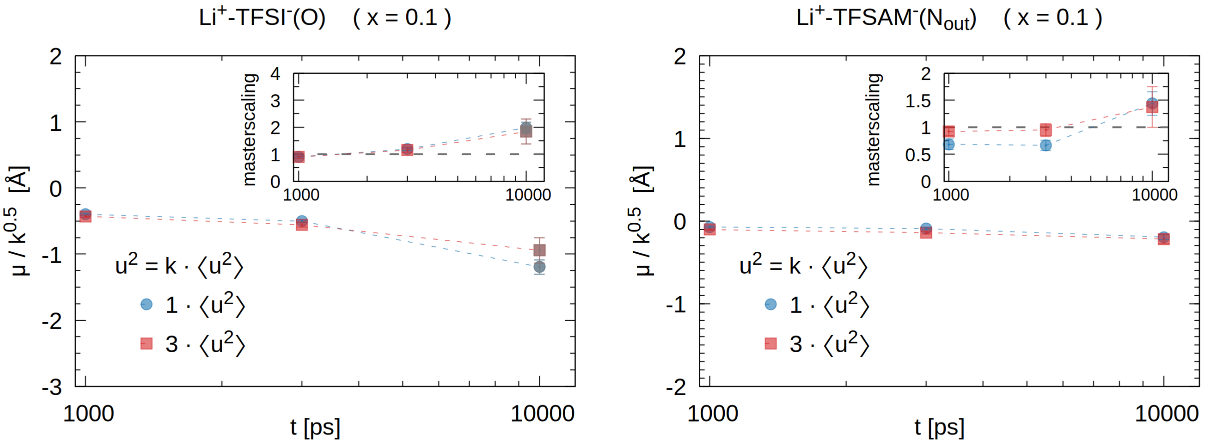

Figure S16: Scaling relations exemplary for the direct anion binding sites TFSI$^-$(O) and TFSAM$^-$(N$_{\mathrm{mid}}$) at a low salt content of x = 0.1: Gaussian peak positions $\mu(t)$ divided by the square root of the distance scaling factor k. Inset: Masterscaling of the Gaussian peak parameters μ and σ^2 to 1 according to Equation SS11. The data points relying on the manually performed Gaussian fits are highlighted in grey. The data points are measured using an upper threshold tolerance $u_{\mathrm{r}}^2 = 1.5 \cdot k \cdot \langle u^2 \rangle$.

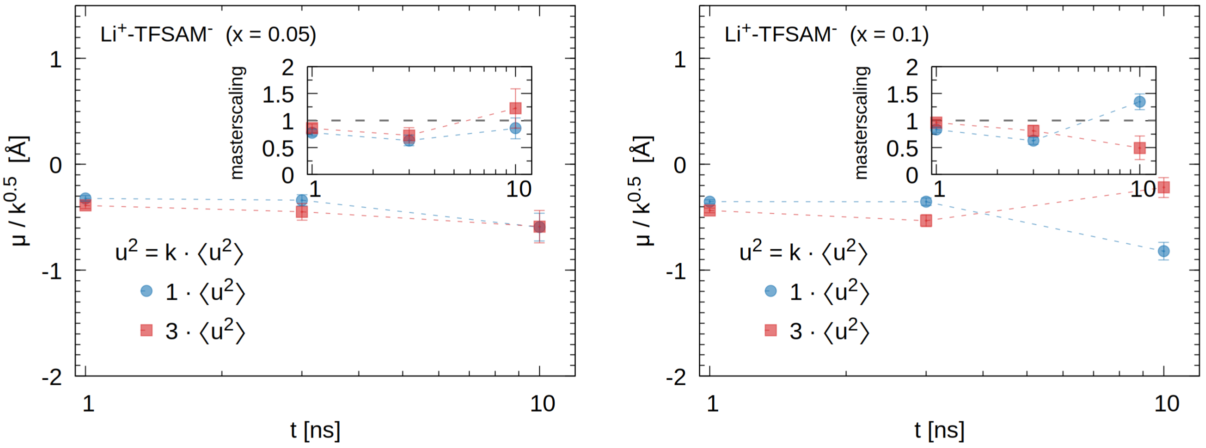

Figure S17: Scaling relations exemplary for the TFSAM$^-$-based mixtures for x = 0.05 and 0.1 using an upper threshold tolerance $u_{\mathrm{r}}^2 = 1.3 \cdot k \cdot \langle u^2 \rangle$.

H: Quantification of dynamically decoupled anions p_{lost}

The ratio of dynamically decoupled anions is estimated from the relative displacement distribution by subtracting the Gaussian peak fit $\mathcal{N}(\mu, \sigma^2)$ from the histogram data $p(\Delta v_{\|})$ and summing up the remaining counts: $\int d\Delta v_{\|}(p(\Delta v_{\|}) - \mathcal{N}(\mu, \sigma^2)) \doteq p_{\mathrm{lost}}$. The part of the histogram which is attributed to p_{lost} is highlighted in blue.

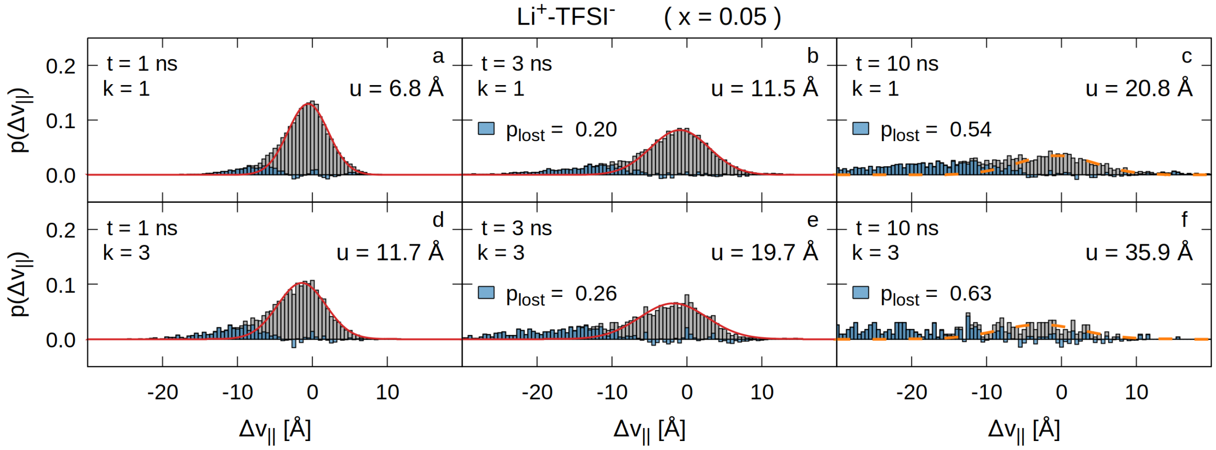

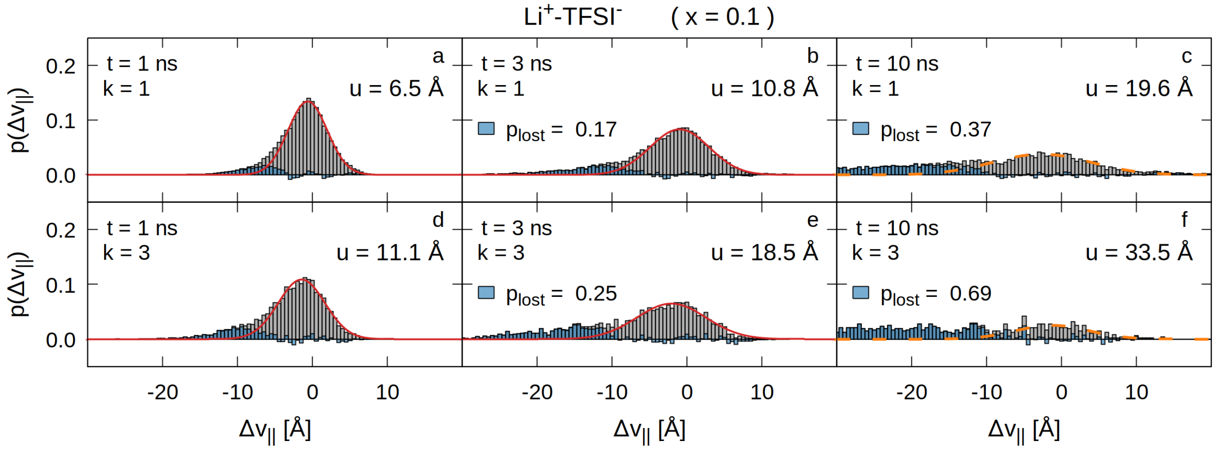

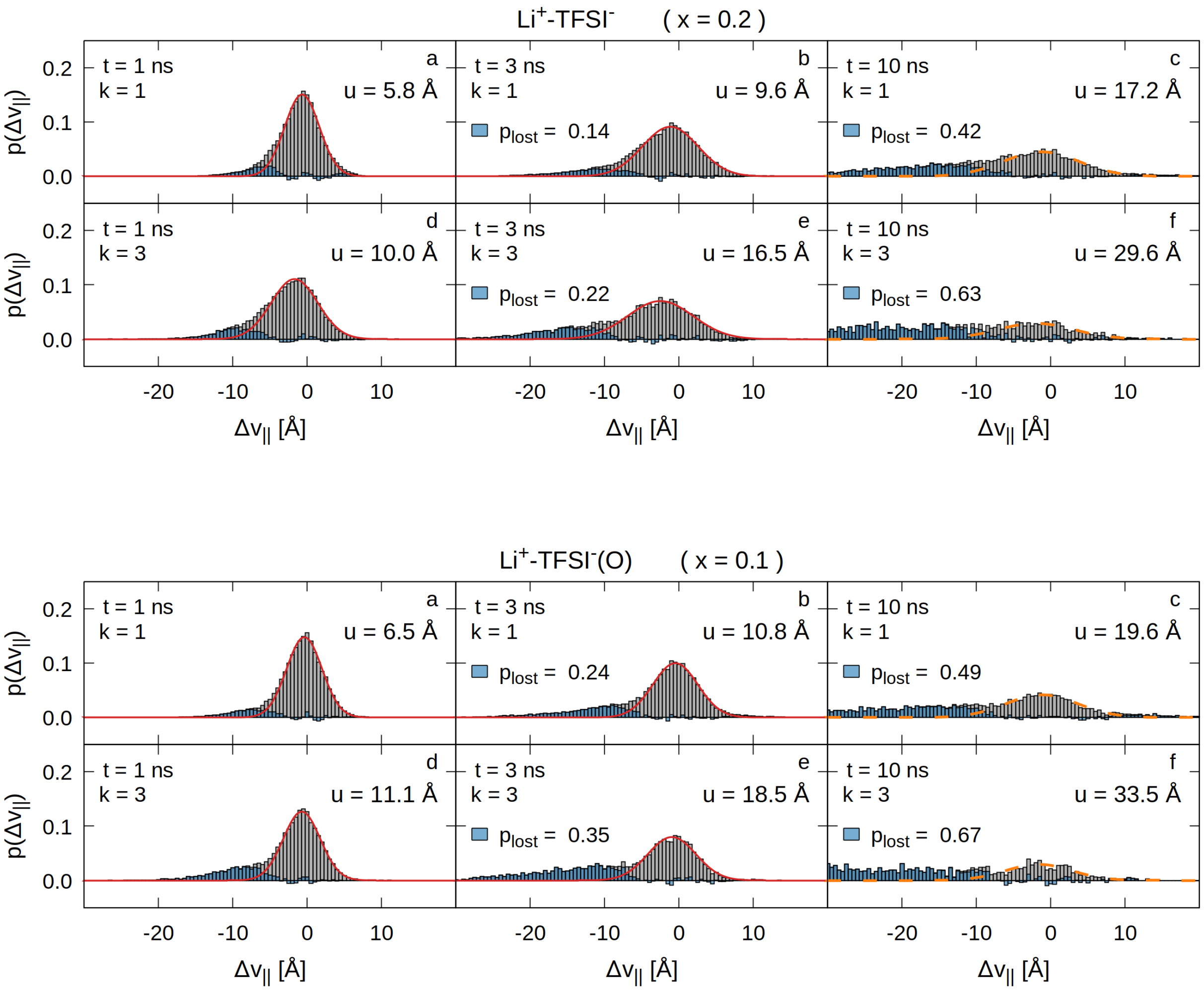

Figure S18: Estimation of the amount p_{lost} of dynamically decoupled TFSI$^-$ shell anions at different lag times t, lithium squared displacements $k \cdot \langle u^2 \rangle$ and various salt contents x. Since the distributions of coupled (Gaussian peak) and decoupled (tail) dynamics overlap considerably at the shortest analysed lag time of $t = 1\,\mathrm{ns}$, a precise quantitative estimate of p_{lost} is not feasible through this procedure.

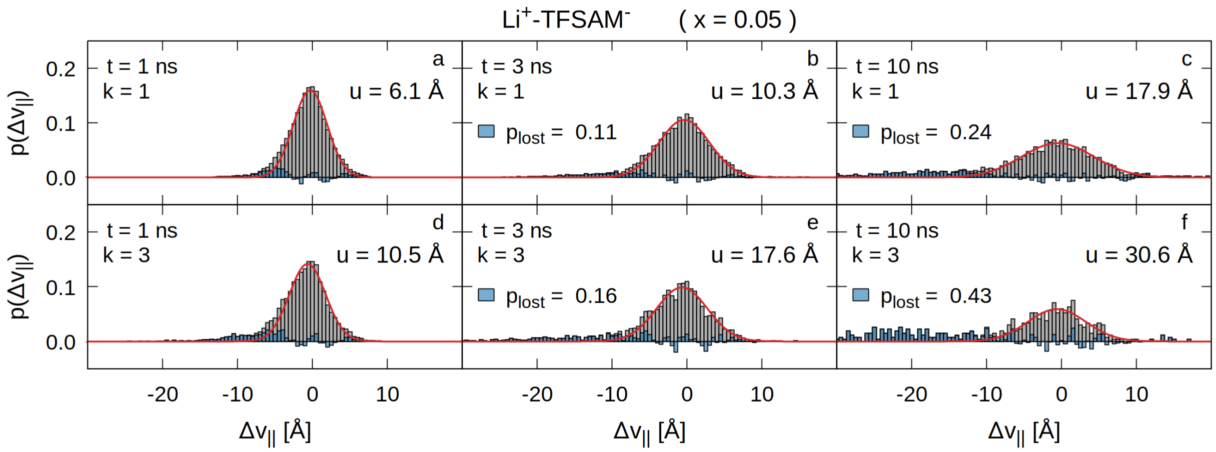
Li+-TFSAM- (x = 0.05)
p(Δv||)
0.2
0.1
0.0
t = 1 ns
k = 1
a
u = 6.1 Å
t = 3 ns
k = 1
b
u = 10.3 Å
plost = 0.11
t = 10 ns
k = 1
c
u = 17.9 Å
plost = 0.24
t = 1 ns
k = 3
d
u = 10.5 Å
t = 3 ns
k = 3
e
u = 17.6 Å
plost = 0.16
t = 10 ns
k = 3
f
u = 30.6 Å
plost = 0.43
-20
-10
0
10
Δv|| [Å]

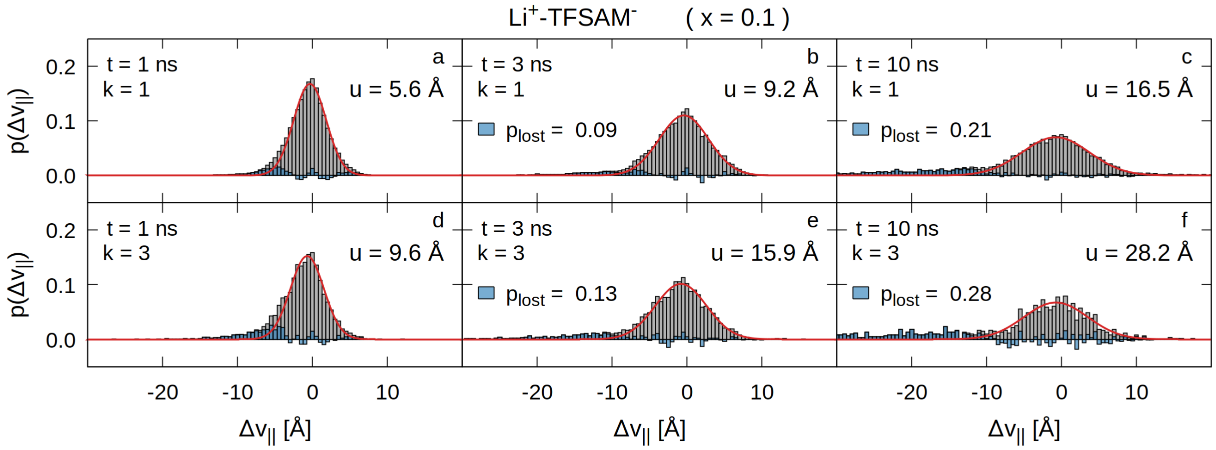
Li+-TFSAM- (x = 0.1)
p(Δv||)
0.2
0.1
0.0
t = 1 ns
k = 1
a
u = 5.6 Å
t = 3 ns
k = 1
b
u = 9.2 Å
plost = 0.09
t = 10 ns
k = 1
c
u = 16.5 Å
plost = 0.21
t = 1 ns
k = 3
d
u = 9.6 Å
t = 3 ns
k = 3
e
u = 15.9 Å
plost = 0.13
t = 10 ns
k = 3
f
u = 28.2 Å
plost = 0.28
-20
-10
0
10
Δv|| [Å]

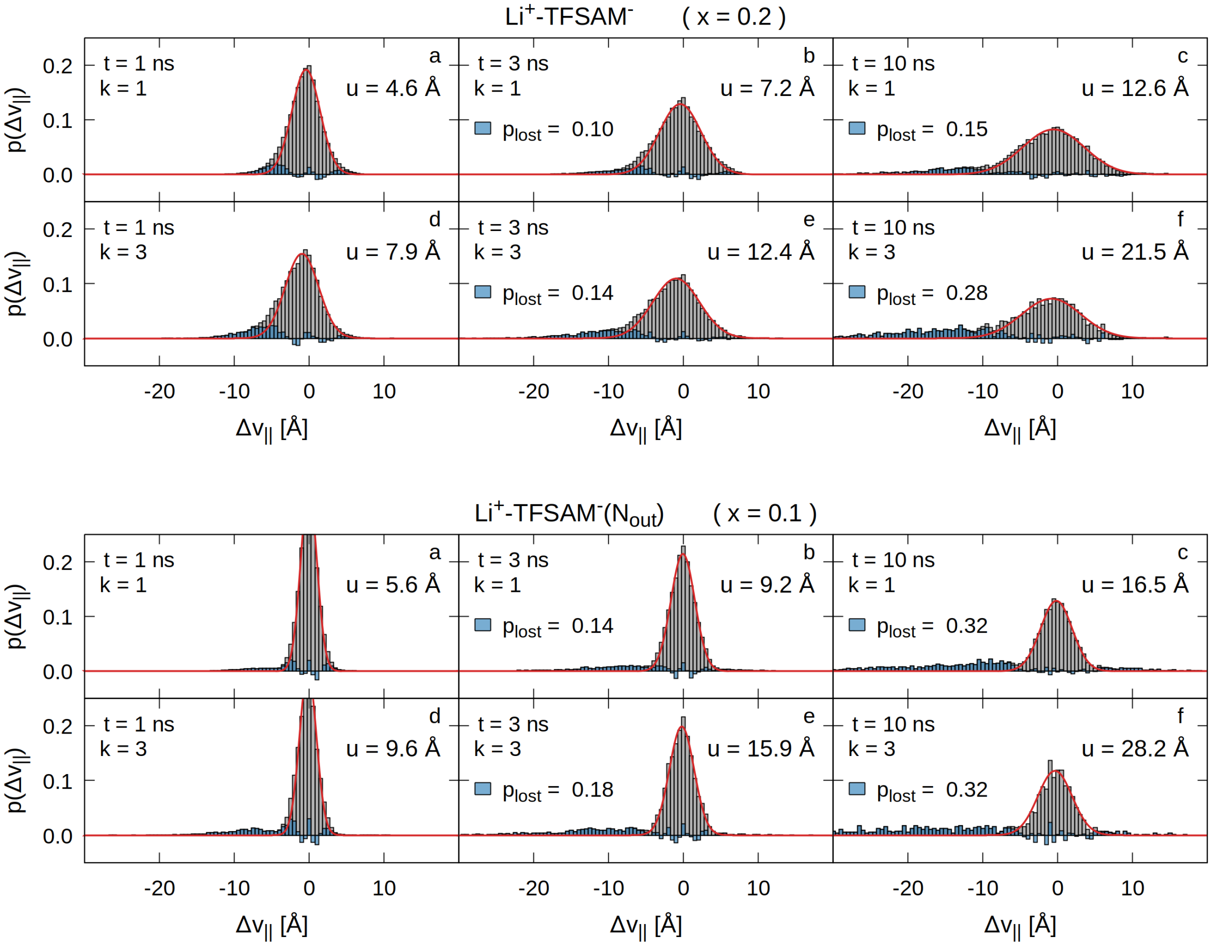

Figure S19: Estimation of the amount p_{lost} of dynamically decoupled TFSAM$^-$ shell anions at different lag times t, lithium squared displacements $k \cdot \langle u^2 \rangle$ and various salt contents x. Since the distributions of coupled (Gaussian peak) and decoupled (tail) dynamics overlap considerably at the shortest analysed lag time of $t = 1\,\text{ns}$, a precise quantitative estimate of p_{lost} is not feasible through this procedure.

I: LCF λ as a function of squared lithium displacement $u^2(t)$

The Li^+ coupling factor λ, which measures the extent to which an initially lithium-bound anion follows the dynamics of this very Li^+, is binned according to the squared displacement u^2 of this Li^+. The data sets are generated by averaging over multiple individual blocks, *e.g.*, the 400 ns trajectories are divided into 130 blocks to evaluate the lag time t $=$ 3 ns.

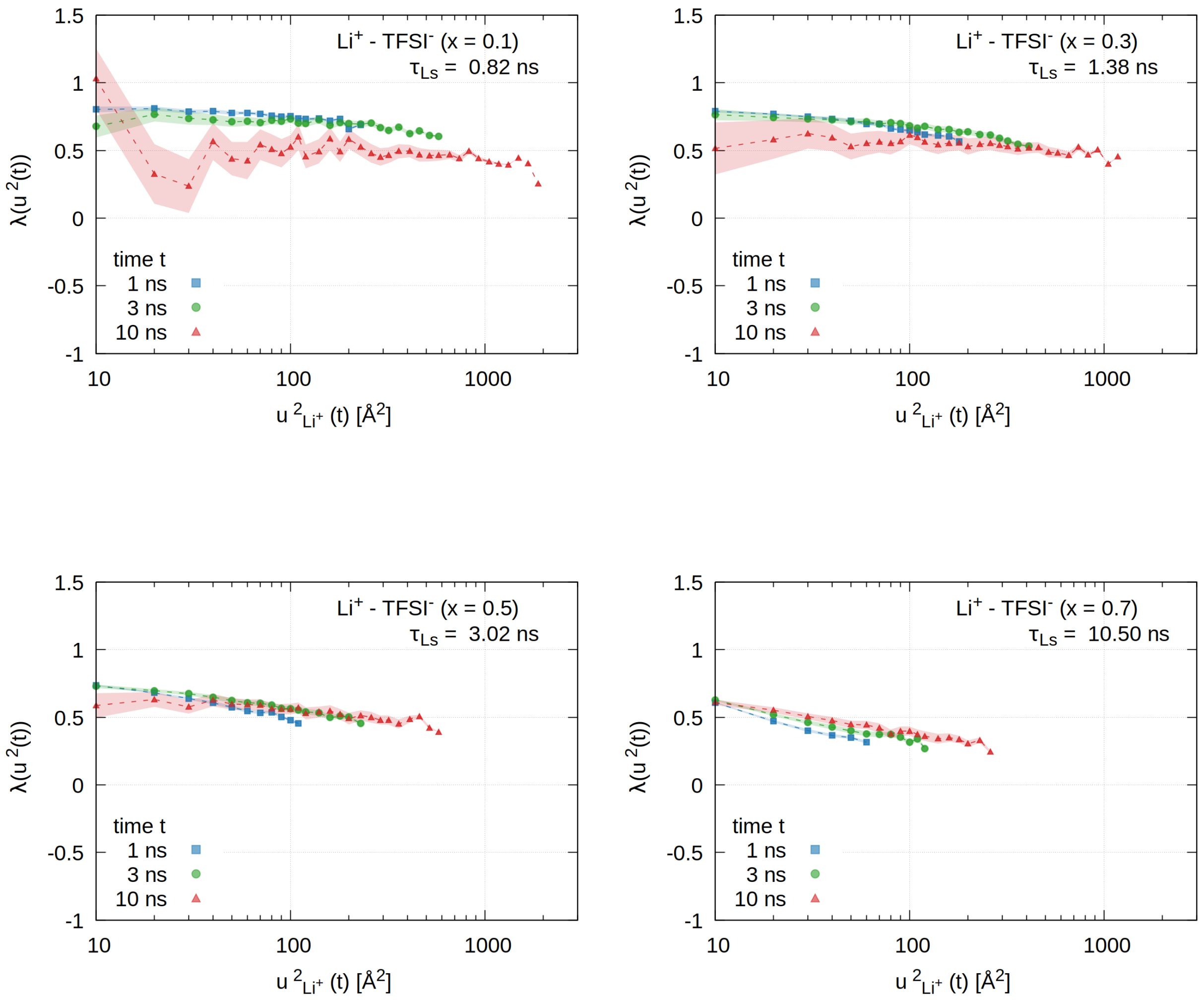

Figure S20: Coupling of anion motion to lithium dynamics measured via λ as a function of $u^2(\mathrm{t})_{\mathrm{Li}^+}$ exemplary for the lithium salt fractions $\mathrm{x} = 0.1$, 0.3, 0.5 and 0.7 in the TFSI^--containing mixtures.

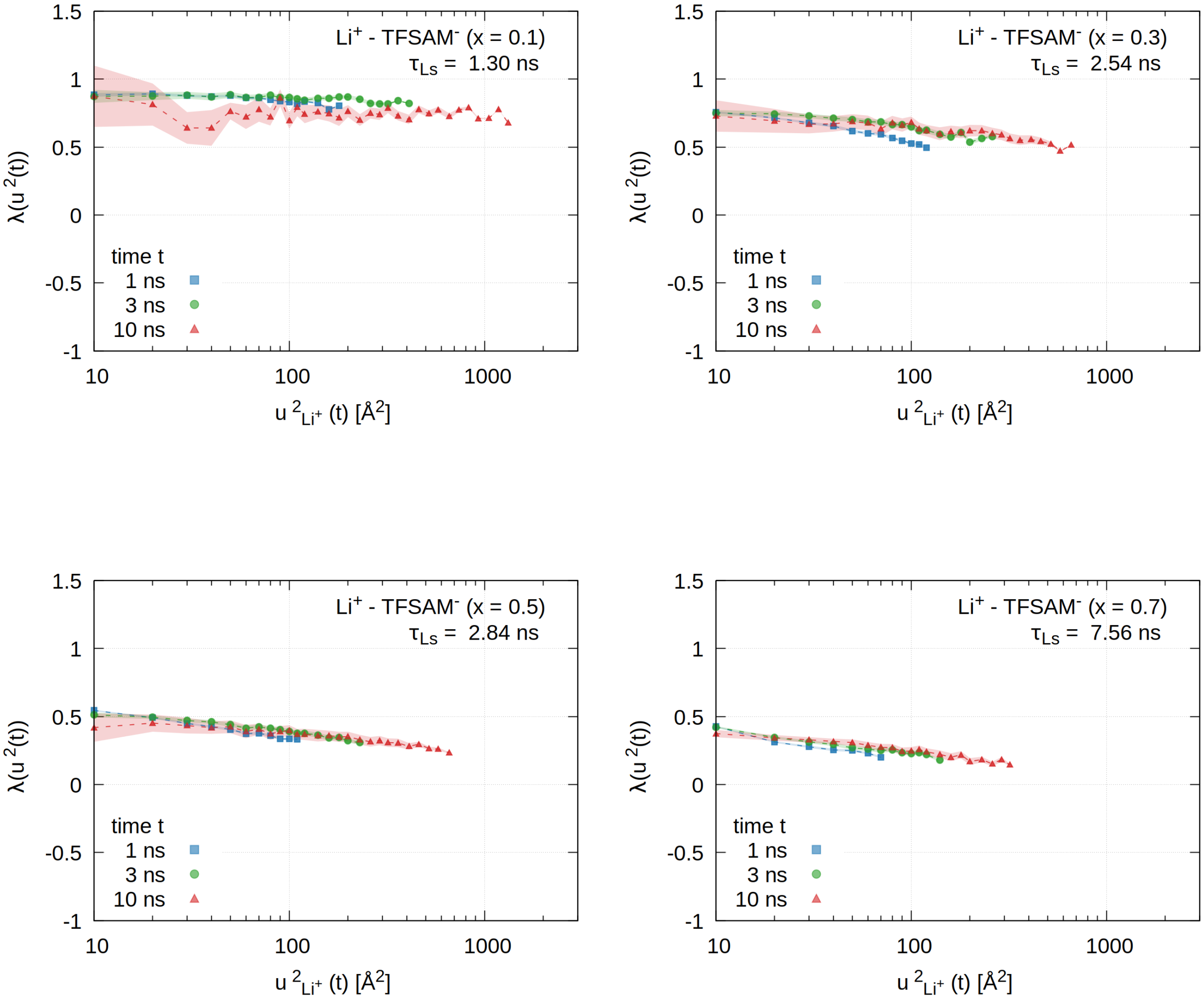

Figure S21: Coupling of anion motion to lithium dynamics measured via λ as a function of $u^2(\mathrm{t})_{\mathrm{Li}^+}$ exemplary for the lithium salt fractions x = 0.1, 0.3, 0.5 and 0.7 in the TFSAM$^-$-containing mixtures.

J: $\vec{\epsilon}^2$, $\vec{\epsilon}_{\parallel}^2$ and $\vec{\epsilon}_{\perp}^2$ as a function of squared lithium displacement $u^2(t)$

One may split the random motion $\vec{\epsilon}$ of an anion into contributions parallel and orthogonal to the lithium path direction $\hat{r} = \vec{u}\,/\,|\,\vec{u}\,|$, which can be computed as

$$\begin{aligned} \vec{\epsilon} &= \vec{v} - \lambda_{u^2} \cdot \vec{u} \\ \vec{\epsilon}_{\parallel} &= (\vec{\epsilon} \cdot \hat{r}) \cdot \hat{r} \\ \vec{\epsilon}_{\perp} &= \vec{\epsilon} - \vec{\epsilon}_{\parallel}. \end{aligned} \tag{S12}$$

λ_{u^2} corresponds to the definition in Equation 7 in the main manuscript $\lambda(u^2, t) = \dfrac{\langle\, \vec{u}_i \cdot \vec{v}_j^{\,i} \,\rangle_{u^2,t}}{u^2} = \dfrac{\langle v_{\parallel} \rangle_{u^2,t}}{u}$, *i.e.*, the data shown in Figures S20 and S21.

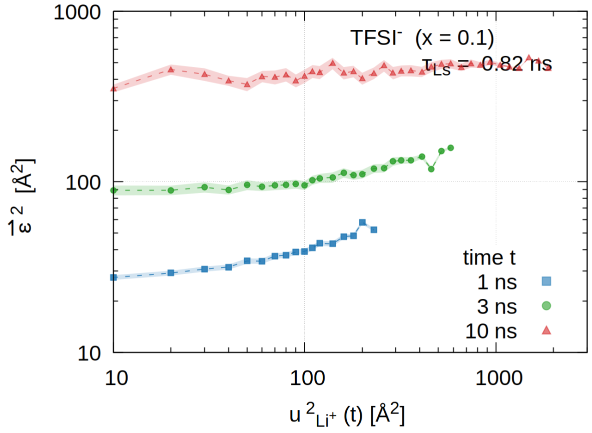

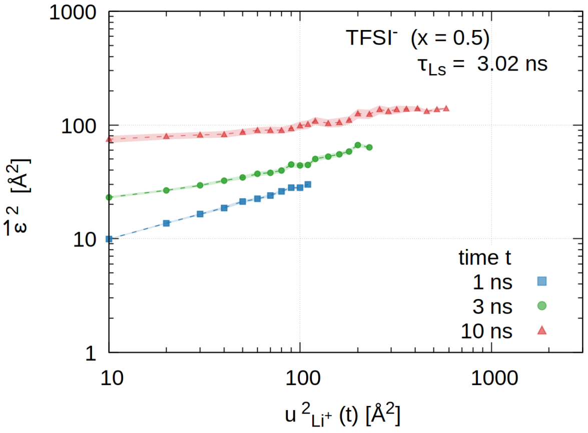

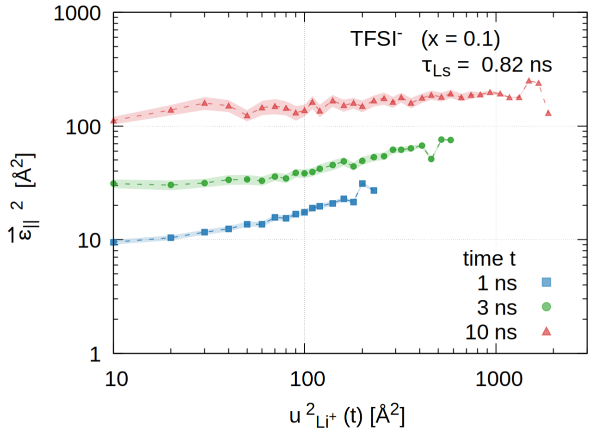

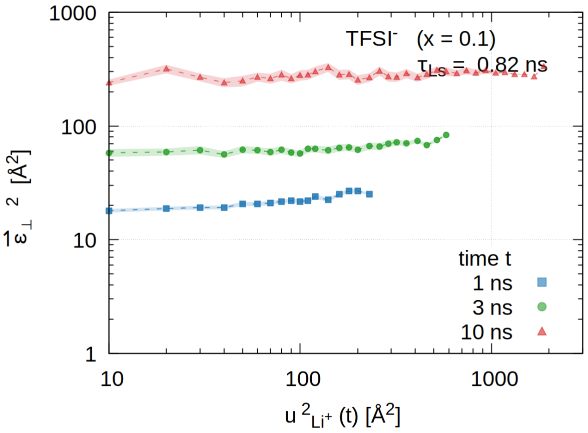

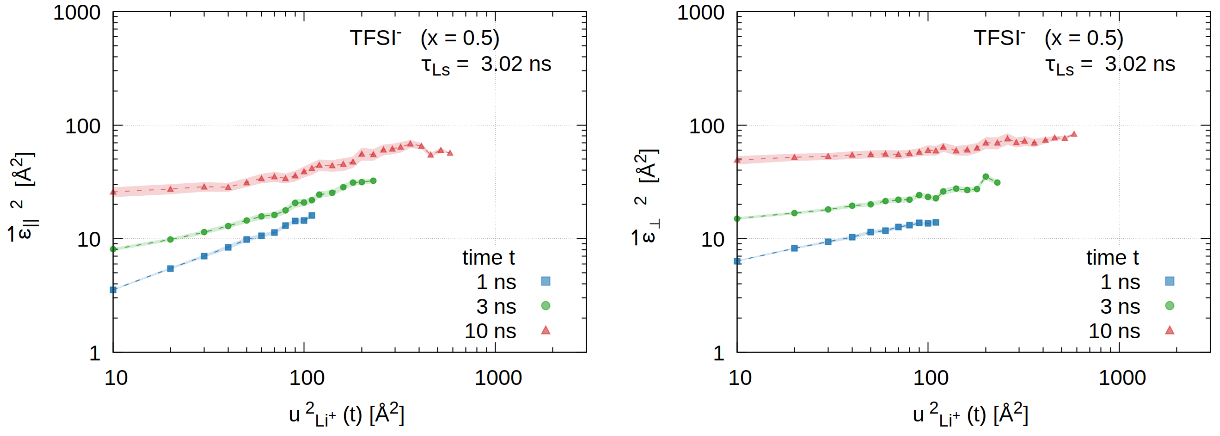

Figure S22: Variances $\vec{\epsilon}^2$, $\vec{\epsilon}_{\|}^2$ and $\vec{\epsilon}_{\perp}^2$ as a function of $u^2(\mathrm{t})_{\mathrm{Li}^+}$ for TFSI$^-$ exemplary for salt contents x = 0.1 and x = 0.5.

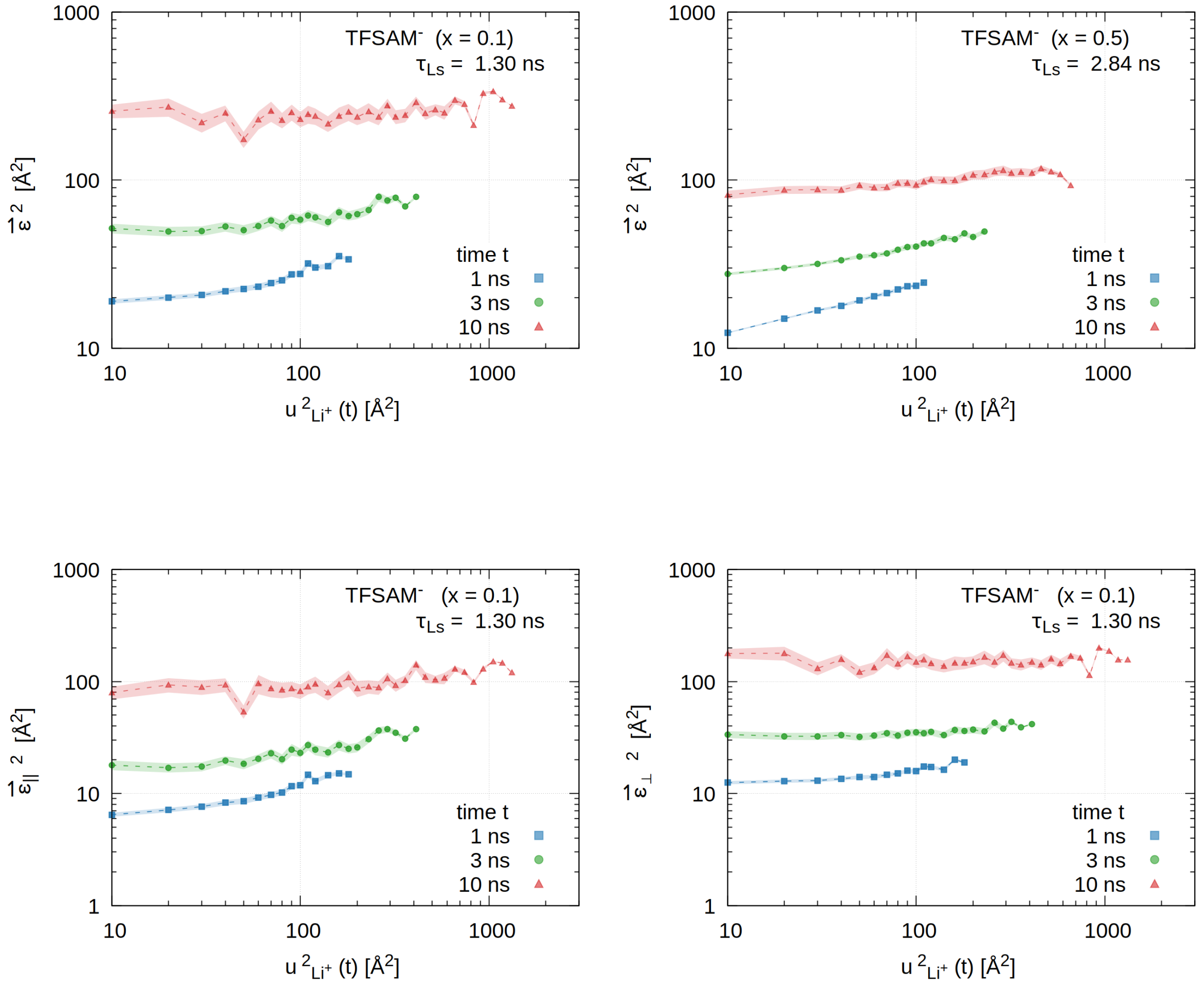

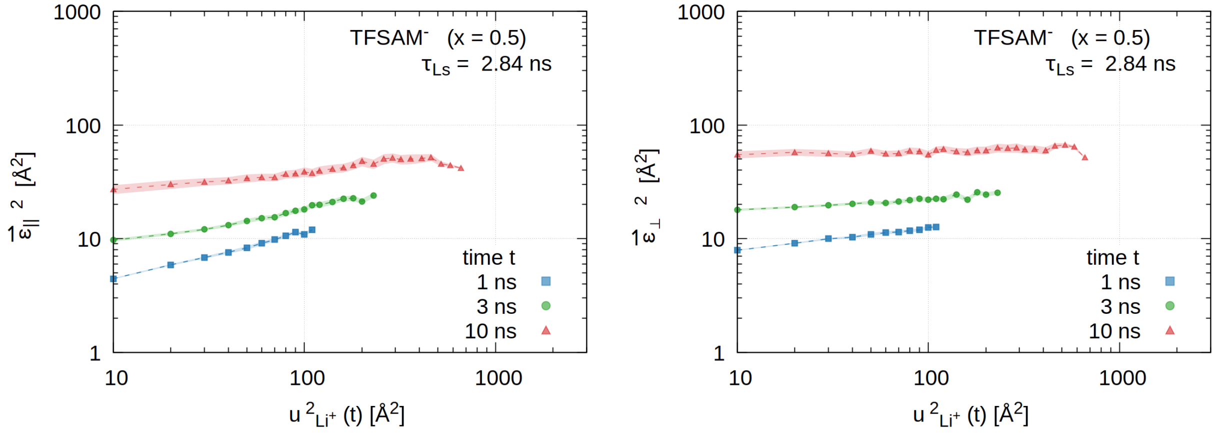

Figure S23: Variances $\vec{\epsilon}^2$, $\vec{\epsilon}_{\parallel}^2$ and $\vec{\epsilon}_{\perp}^2$ as a function of $u^2(\mathrm{t})_{\mathrm{Li}^+}$ for TFSAM$^-$ exemplary for salt contents x = 0.1 and x = 0.5.

K: Correlation of the random motion of next-neighbor anions in a solvation shell

To investigate the interaction between two initially adjacent anions anion$_1$ and anion$_2$ in a lithium solvation shell, we compute the correlation $(\vec{\epsilon}_1 \cdot \vec{\epsilon}_2)/(\vec{\epsilon}^2)$ as well as quantify the contributions parallel $\left(\vec{\epsilon}_{1,\parallel} \cdot \vec{\epsilon}_{,\parallel}\right)/(\vec{\epsilon}_{\parallel}^2)$ and orthogonal $\left(\vec{\epsilon}_{1,\perp} \cdot \vec{\epsilon}_{,\perp}\right)/(\vec{\epsilon}_{\perp}^2)$ to the lithium pathway.

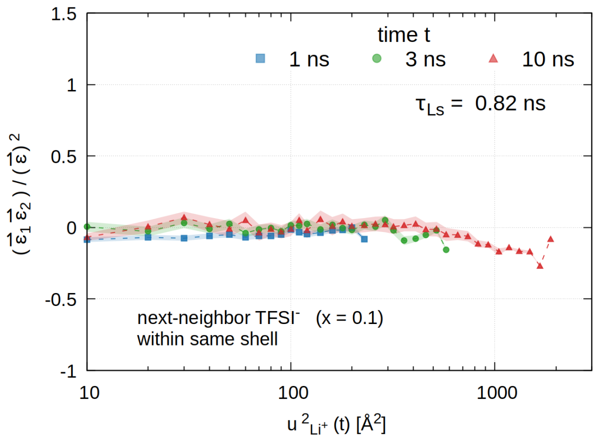

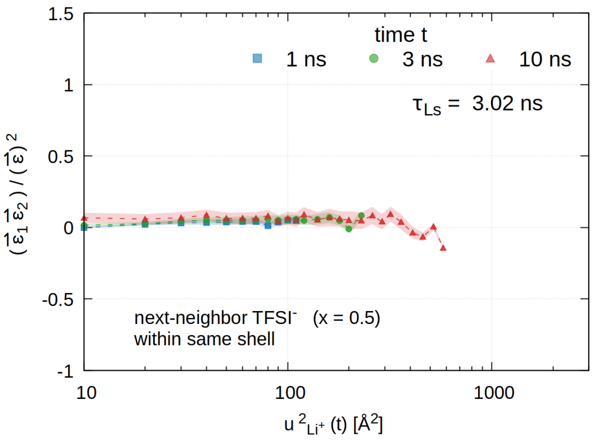

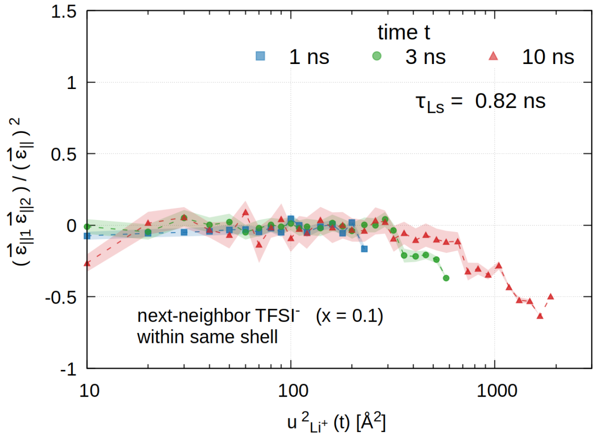

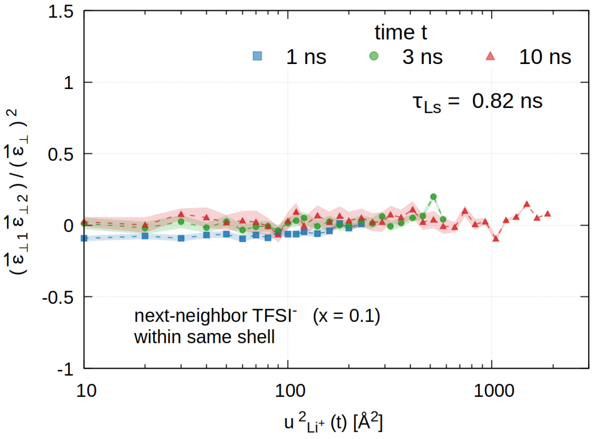

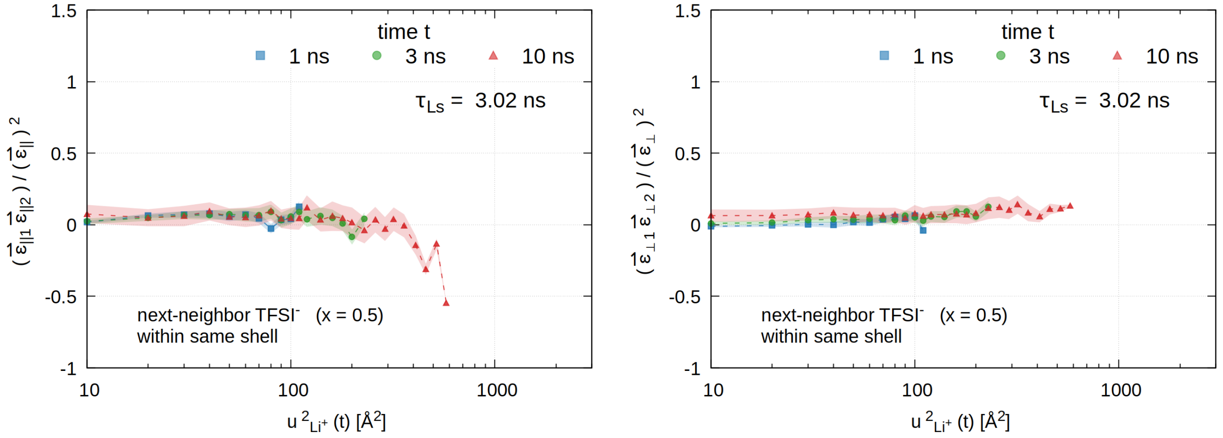

Figure S24: Correlations of initial next-neighbor shell anions TFSI$_1^-$ and TFSI$_2^-$ as a function of $u^2(\mathrm{t})_{\mathrm{Li}^+}$ exemplary for salt contents $\mathrm{x} = 0.1$ and $\mathrm{x} = 0.5$.

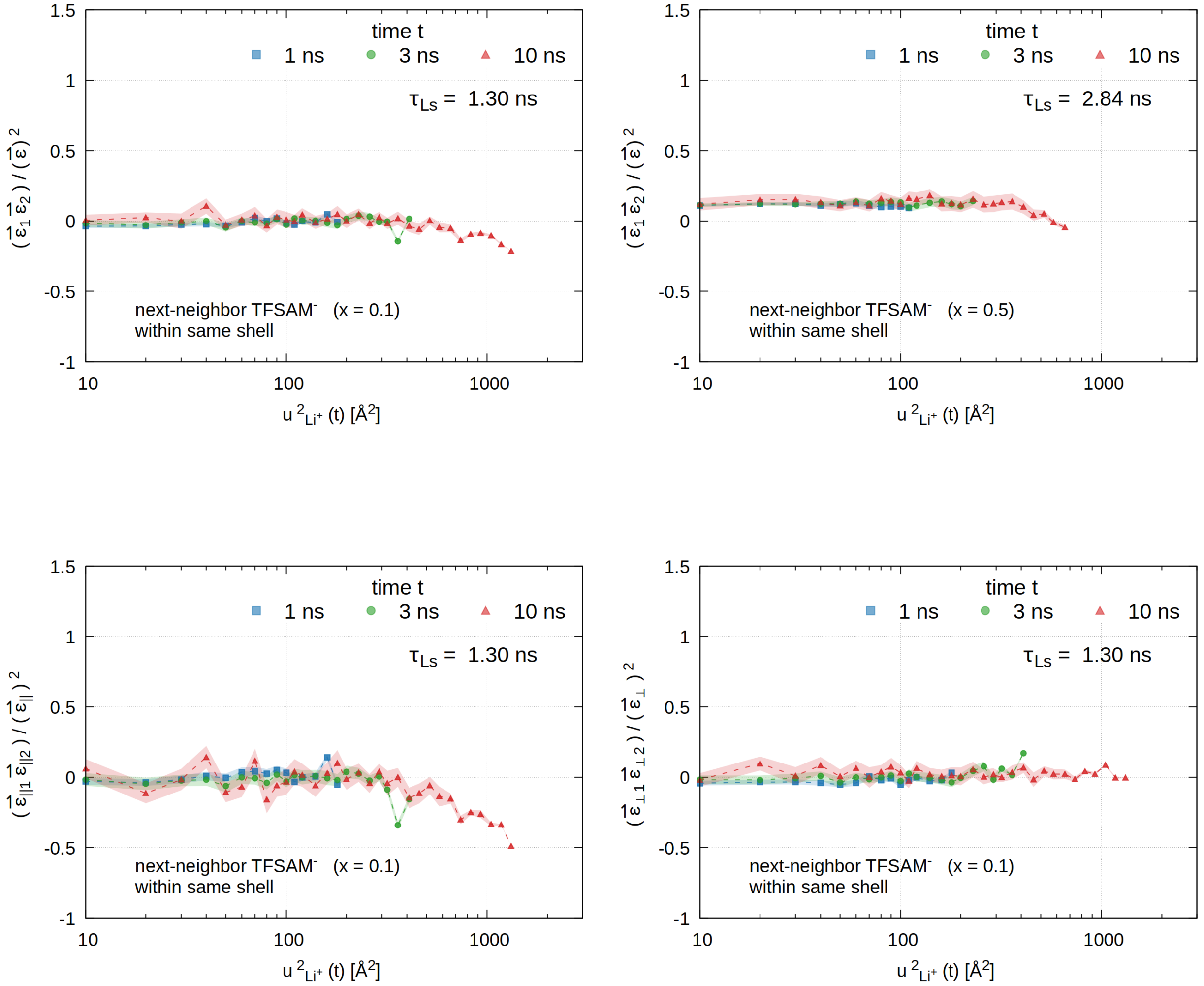

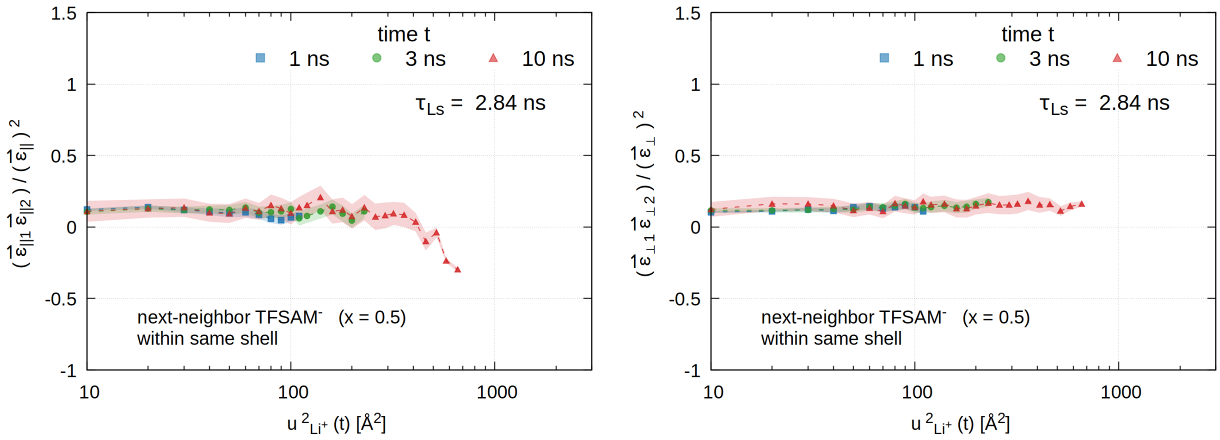

Figure S25: Correlations of initial next-neighbor shell anions TFSAM_1^- and TFSAM_2^- as a function of $u^2(\mathrm{t})_{\mathrm{Li}^+}$ exemplary for salt contents $\mathrm{x} = 0.1$ and $\mathrm{x} = 0.5$.

L: LCF λ as a function of time t

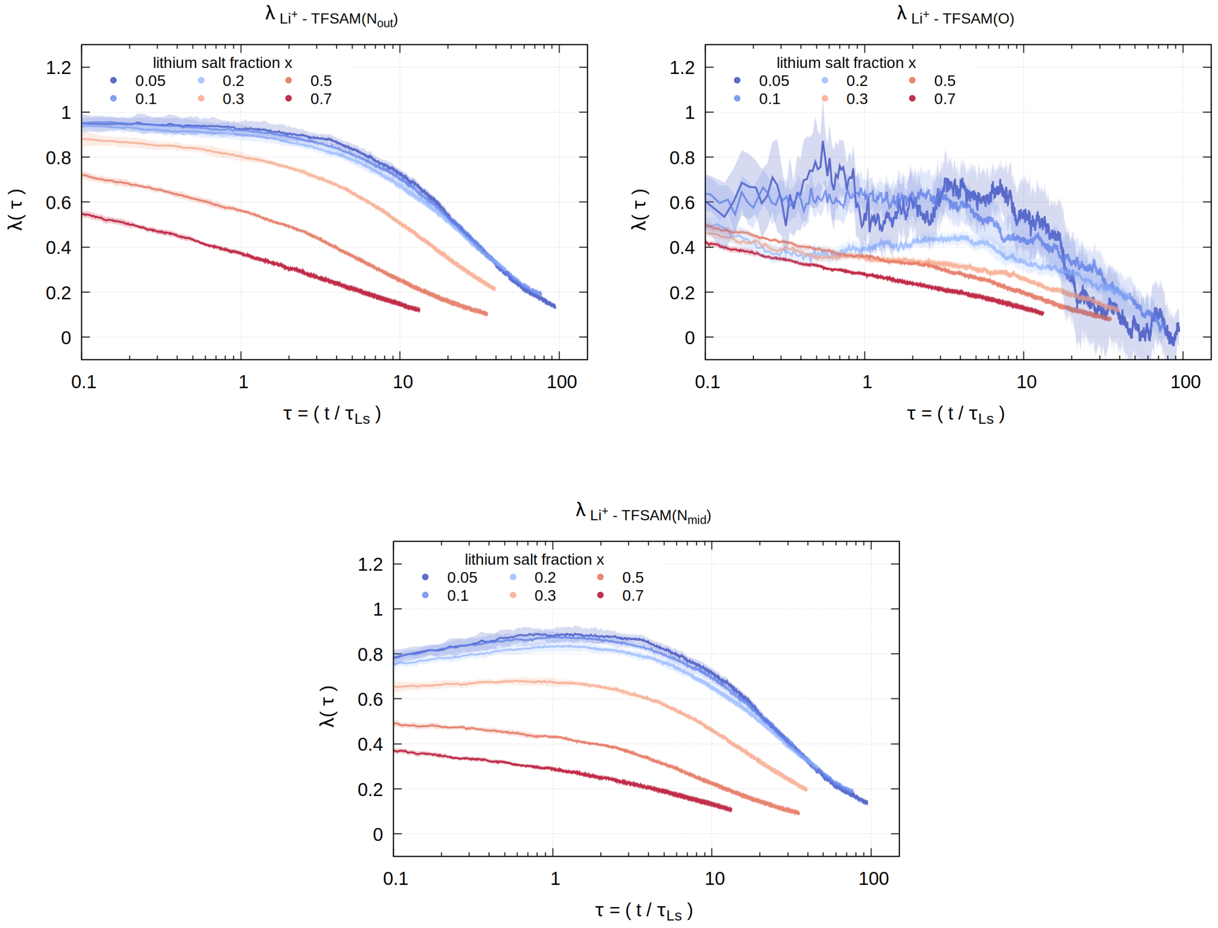

Figure S26: Time dependence of LCF λ for Li^+ to different binding sites provided by $TFSAM^-$, *i.e.*, the outer nitrogen atoms N_{out} (top left) or the oxygen atoms (top right). Using the second minimum position of $g_{Li^+-N_{mid}}$ as a cutoff distance to determine $Li^+ - TFSAM^-$-binding as discussed in the manuscript, contains all possible coordination geometries. For a structurally equivalent comparison with $TFSI^-$, we analyse the LCF of Li^+ and the middle nitrogen atoms N_{mid} in the initial $TFSAM^-$ solvation cage. To compare the time dependence of λ for different salt contents x, t is scaled by the characteristic self diffusion time τ_{Ls} (see Figure 5B) of each electrolyte composition.

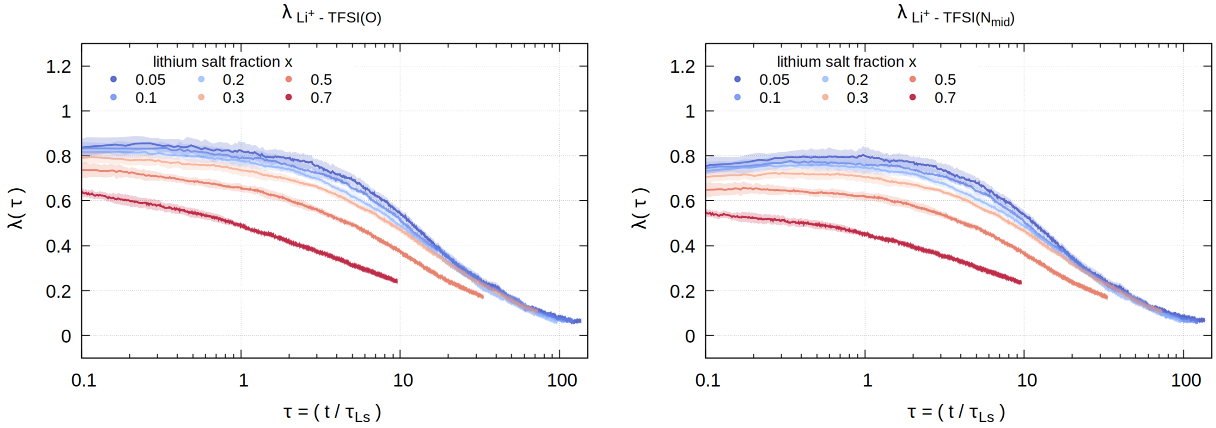

Figure S27: Time dependence of LCF λ for Li^+ to the oxygen atoms (top left) of TFSI^-. Employing the second minimum position of $g_{\mathrm{Li}^+-\mathrm{N}_{\mathrm{mid}}}$ as a cutoff distance to determine Li^+ – TFSI^--binding as discussed in the main manuscript allows for a structurally equivalent comparison with TFSAM^-. Thus, we analyse the LCF of Li^+ and the middle nitrogen atoms $\mathrm{N}_{\mathrm{mid}}$ in the initial TFSI^- solvation cage. To compare the time dependence of λ for different salt contents x, t is scaled by the characteristic self diffusion time τ_{Ls} (see Figure 5A) of each electrolyte composition.

M: Comparison of $\lambda, \lambda_1, \lambda_2$ and Λ_2 as a function of salt content x for characteristic times of $3 \cdot \tau_{\mathbf{Ls}}$ and $5 \cdot \tau_{\mathbf{Ls}}$

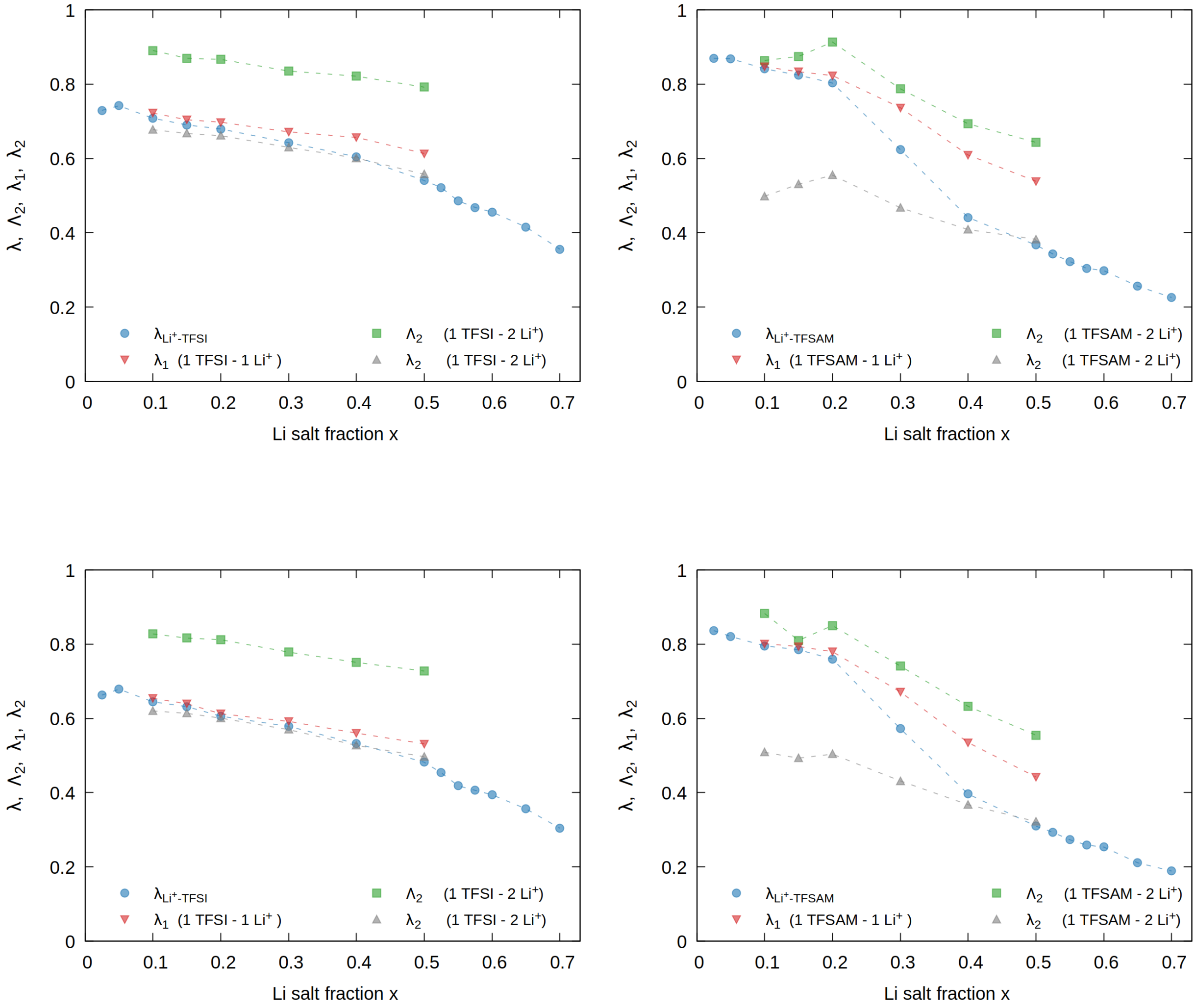

Figure S28: Comparison of lithium coupling factors $(\lambda, \lambda_1, \lambda_2, \Lambda_2)$ as a function of salt content for both TFSI$^-$ (left) and TFSAM$^-$ (right) - based mixtures for characteristic times of $3 \cdot \tau_{\mathrm{Ls}}$ (top) and $5 \cdot \tau_{\mathrm{Ls}}$ (bottom).

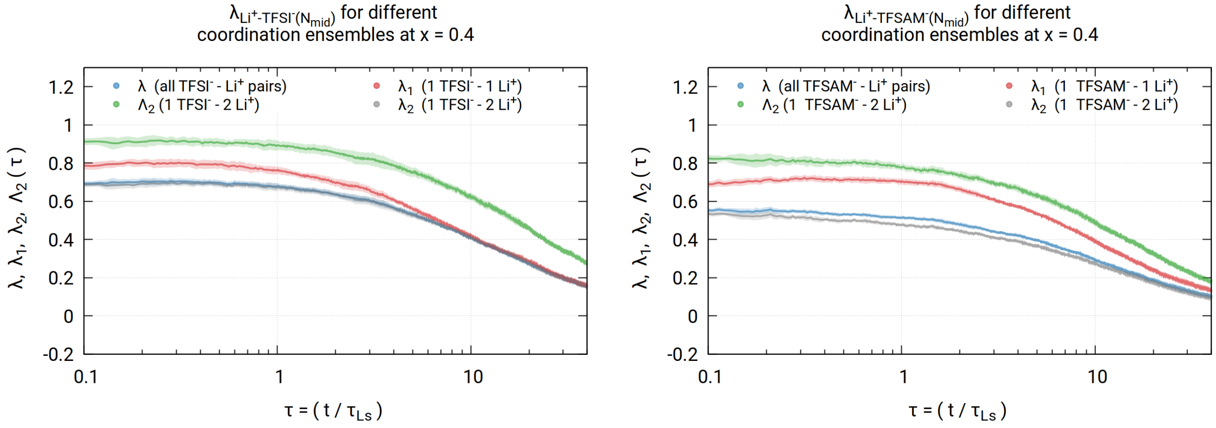

Figure S29: Time dependence of LCF λ, λ_1, λ_2 and Λ_2 exemplary shown for the x=0.4 TFSI$^-$-(left) and TFSAM$^-$-based (right) electrolyte compositions.

N: Additional information for discussing $\mathbf{D_{anion}/D_{Li^+}}$ as a function of salt content x

It can be easily shown that the line of argumentation for a decreasing ratio $\langle\vec{v}\rangle/\langle\vec{u}\rangle$ as a consequence of double Li$^+$-anion coordination is applicable to higher Li$^+$ over-coordination of the anion. Assume the anion j is bound to n Li$^+$ and tries to couple with the strength Λ_n to the average Li$^+$ displacement $\vec{U}_i^j = \frac{1}{n}\cdot(\vec{u}_1 + ... + \vec{u}_n)$:

$$\vec{v}_j = \Lambda_n \cdot \vec{U}_i^j + \vec{E}_j. \tag{S13}$$

Squaring and rearranging yields for the ratio $\langle\vec{v}\rangle/\langle\vec{u}\rangle$:

$$\begin{aligned}\frac{\langle\vec{v}^2\rangle}{\langle\vec{u}\rangle} &= \Lambda_n^2 \cdot \frac{1}{n^2} \cdot \left(n + 2\binom{n}{2}\frac{\langle\vec{u}_1\vec{u}_2\rangle}{\langle\vec{u}\rangle}\right) + \frac{\vec{E}^2}{\langle\vec{u}\rangle} \\ &= \Lambda_n^2 \underbrace{\cdot \frac{1}{n} \cdot \left(1 + (n-1)\underbrace{\frac{\langle\vec{u}_1\vec{u}_2\rangle}{\langle\vec{u}\rangle}}_{<1}\right)}_{\to\frac{\langle\vec{u}_1\vec{u}_2\rangle}{\langle\vec{u}\rangle}} + \frac{\vec{E}^2}{\langle\vec{u}\rangle}\end{aligned} \tag{S14}$$

If the remaining terms and factors do not change considerably, one can easily see that the ratio drops further with n-fold coordination.

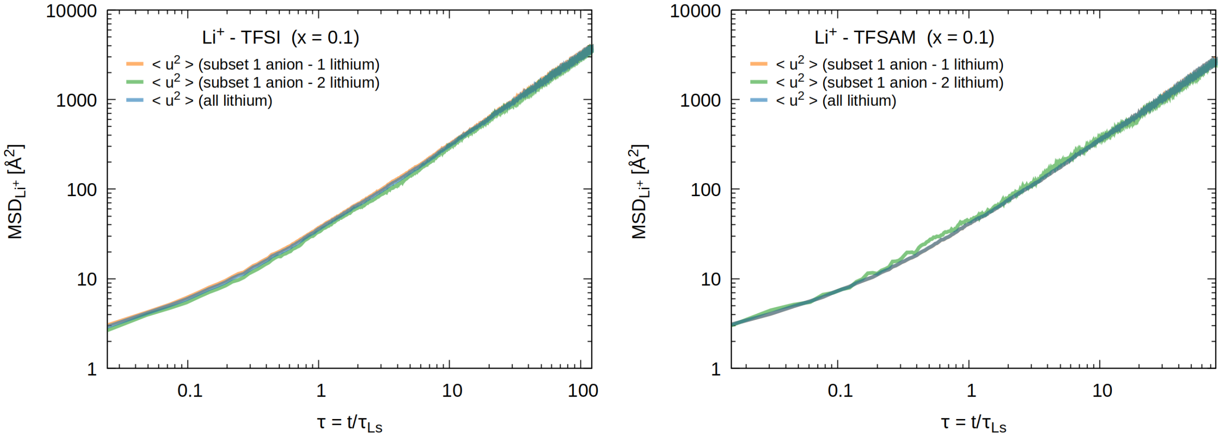

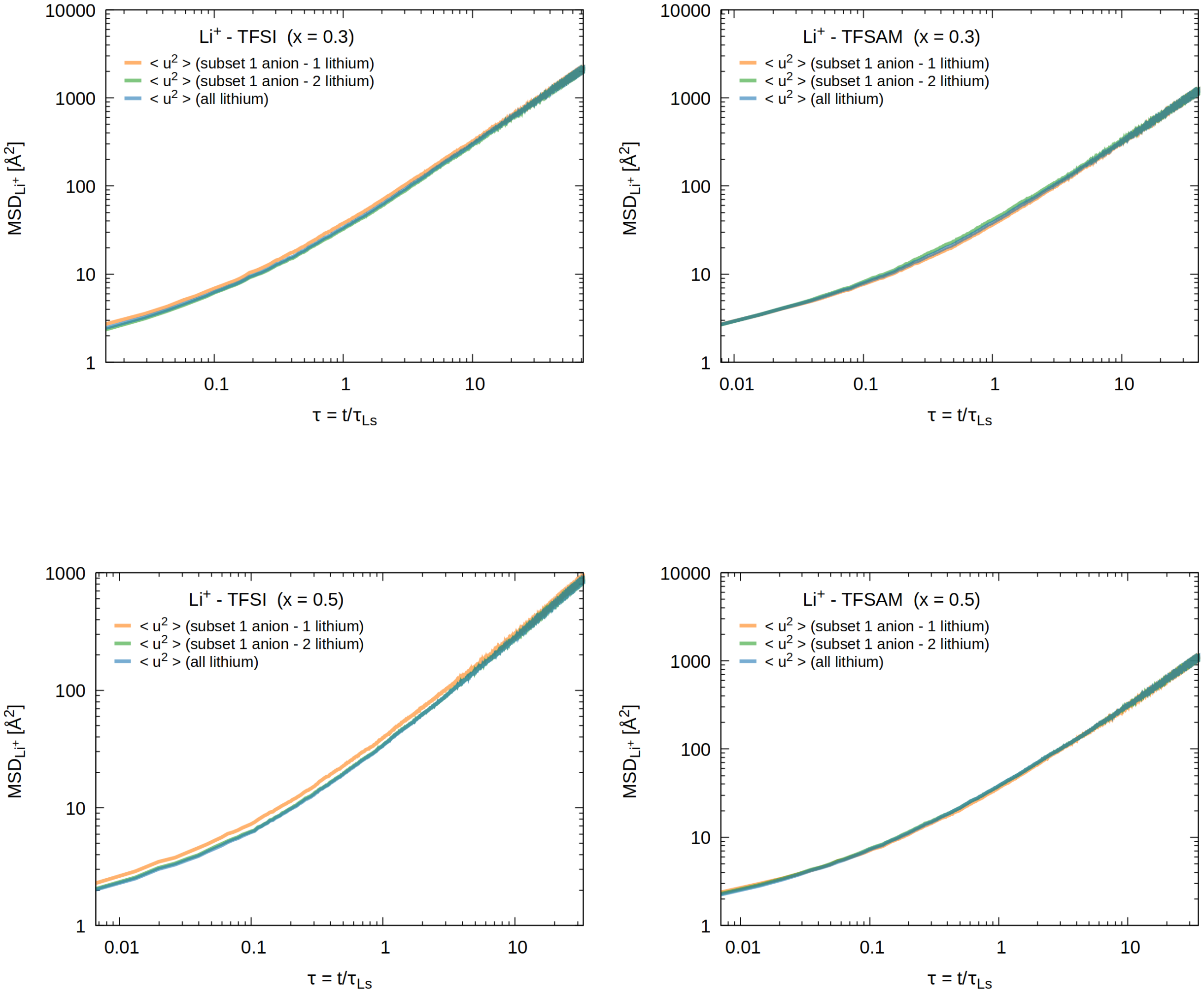

Figure S30: Comparison of lithium MSD to $\langle u^2 \rangle$ in the subensembles of λ_1 and λ_2/Λ_2.

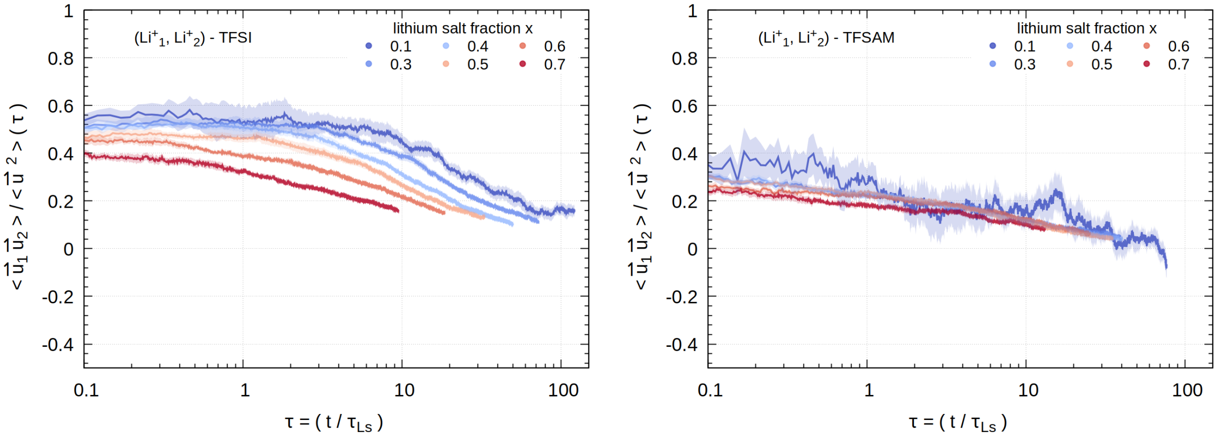

Figure S31: $\mathrm{Li}^+ - \mathrm{Li}^+$ - correlation $\langle \vec{u}_1 \cdot \vec{u}_2 \rangle / \langle \vec{u}^2 \rangle$ for lithium ions that are bound to the same anion at time $\tau = 0$.

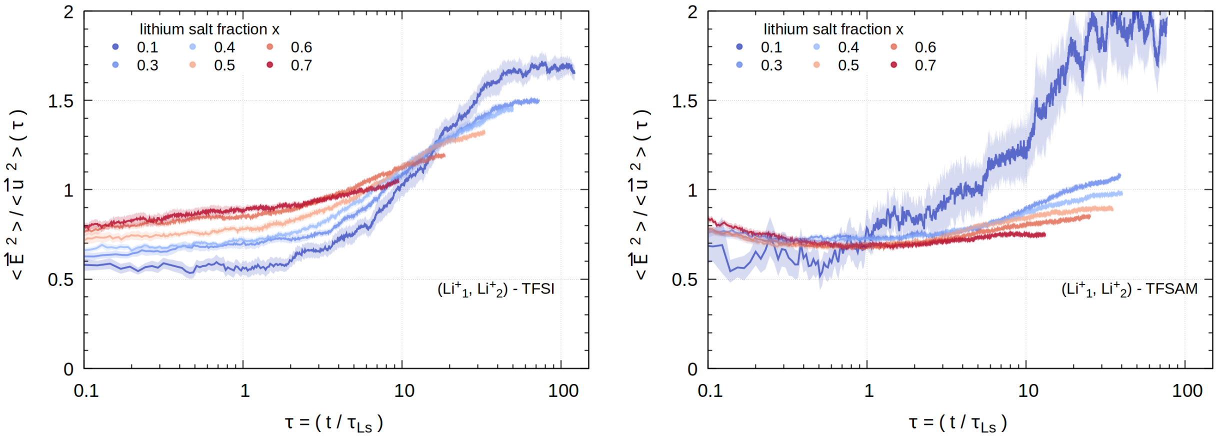

Figure S32: Random motion $\langle \vec{\mathcal{E}}^2 \rangle$ of anions, which have two Li^+ neighbours at time $\tau = 0$, scaled by the average squared lithium displacement $\langle \vec{u}^2 \rangle$. $\langle .. \rangle$ denotes the ensemble average over the Li^+ that are involved in the double coordination of the anion at $\tau = 0$.

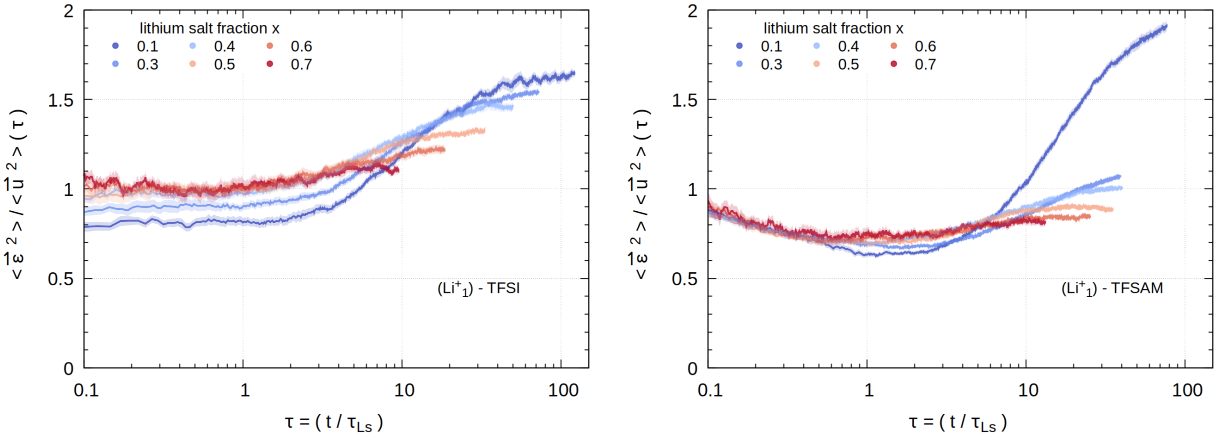

Figure S33: Random motion $\langle\vec{\epsilon}^2\rangle$ of anions, which have only a single Li$^+$ neighbour at time $\tau = 0$, scaled by the average squared lithium displacement $\langle\vec{u}^{\,2}\rangle$. $\langle..\rangle$ denotes the ensemble average over the Li$^+$ that are involved in the single coordination of the anion at $\tau = 0$.

O: Self van Hove function $\mathbf{G_s}(r, \Delta t)$

The self van Hove function $\mathrm{G_s}(r, \Delta t)$ describes the probability distribution that a particle has moved a distance r within a time lag Δt away from its original position:

$$\mathrm{G_s}(r, \Delta t) = \frac{1}{N} \langle \sum_{i=1}^{N} \delta \left(r - |\vec{r}_i(t + \Delta t) - \vec{r}_i(t)| \right) \rangle \tag{S15}$$

Figure S34 gives an overview of the displacement distributions $\mathrm{G_s}(r, \Delta t)$ of the lithium ions at time lags $\Delta t = 10$ ps, 100 ps, 1 ns, 10 ns and 100 ns for the broad spectrum of lithium salt contents. The dashed lines represent the displacement distribution expected for an ideal diffusive motion that exhibits a Gaussian behavior $\mathrm{G_{0,s}}(r, \Delta t) = \left(\frac{3}{2\pi \cdot \langle r^2(\Delta t) \rangle} \right)^{3/2} \exp \left(-\frac{3}{2} \frac{r^2}{\langle r^2(\Delta t) \rangle} \right)$. Comparison of the probed displacement distribution $\mathrm{G_s}(r, \Delta t)$ to $\mathrm{G_{0,s}}(r, \Delta t)$ shows that the non-Gaussian characteristics of the lithium dynamics increase in both electrolyte series with increasing lithium salt content. The tails of the distributions at high displacement distances r are indicative of a fraction of lithium ions that display a higher mobility.

We note that although no secondary peaks emerge in the distributions at elevated salt content, which would indicate that lithium transport is achieved through discrete "hopping" events, the pronounced tails of $\mathrm{G_s}(r, \Delta t)$ might stem from lithium jumps.

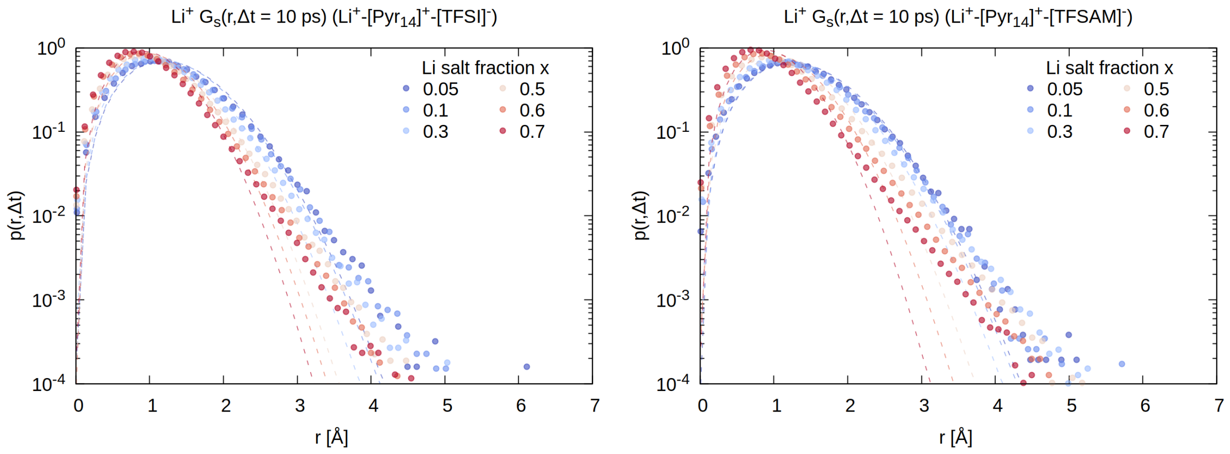

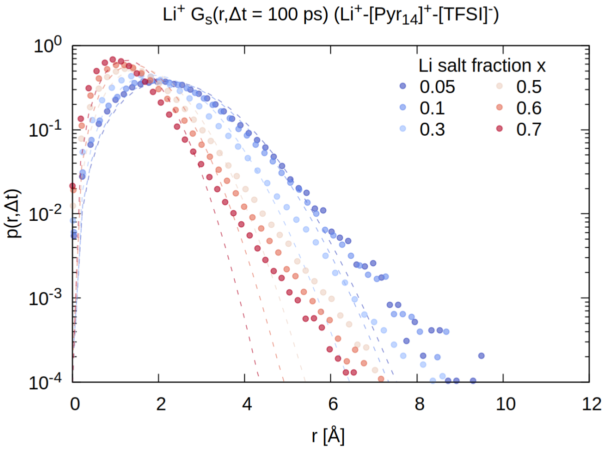
Li$^+$ $G_s(r,\Delta t = 100\text{ ps})$ (Li$^+$-[Pyr$_{14}$]$^+$-[TFSI]$^-$)

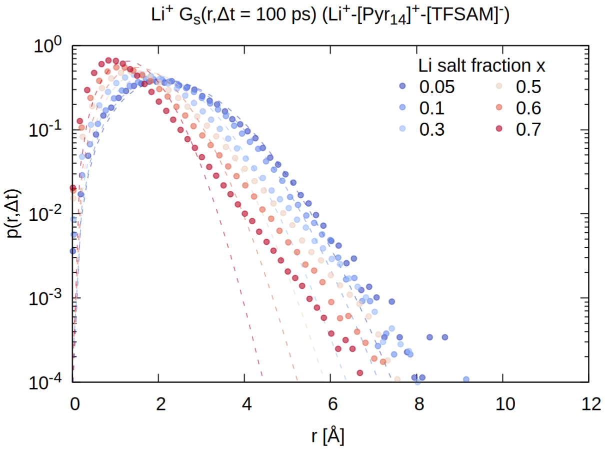
Li$^+$ $G_s(r,\Delta t = 100\text{ ps})$ (Li$^+$-[Pyr$_{14}$]$^+$-[TFSAM]$^-$)

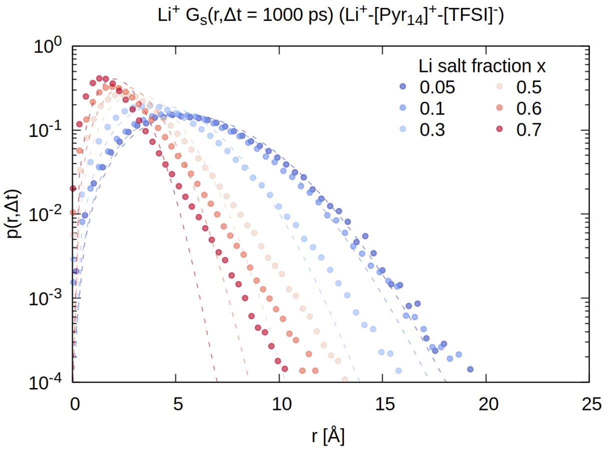
Li$^+$ $G_s(r,\Delta t = 1000\text{ ps})$ (Li$^+$-[Pyr$_{14}$]$^+$-[TFSI]$^-$)

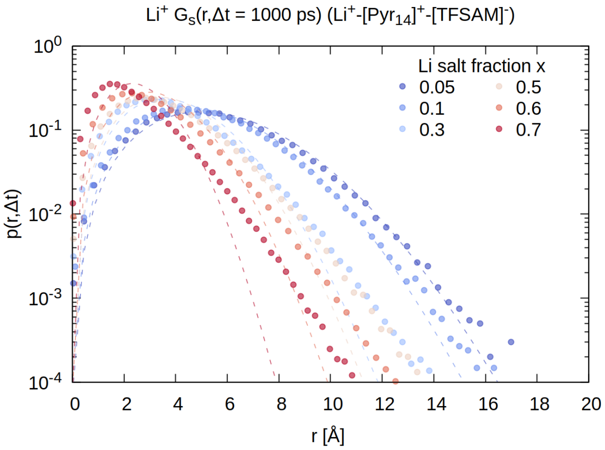
Li$^+$ $G_s(r,\Delta t = 1000\text{ ps})$ (Li$^+$-[Pyr$_{14}$]$^+$-[TFSAM]$^-$)

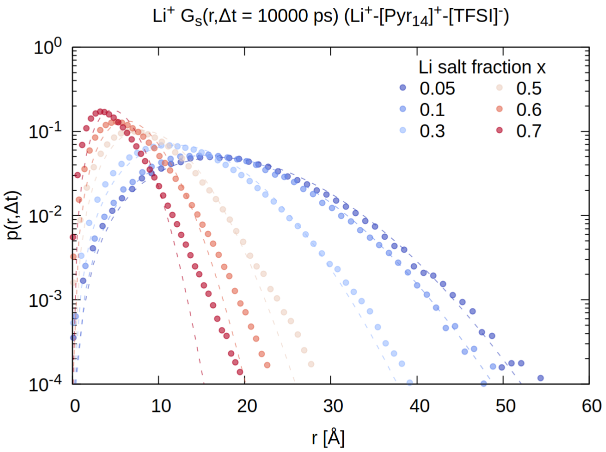
Li$^+$ $G_s(r,\Delta t = 10000\text{ ps})$ (Li$^+$-[Pyr$_{14}$]$^+$-[TFSI]$^-$)

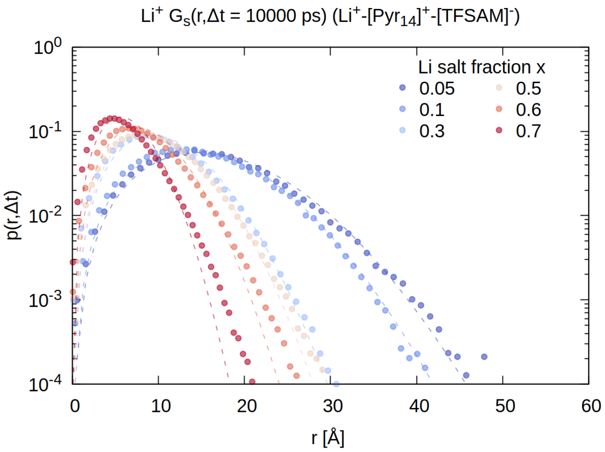
Li$^+$ $G_s(r,\Delta t = 10000\text{ ps})$ (Li$^+$-[Pyr$_{14}$]$^+$-[TFSAM]$^-$)

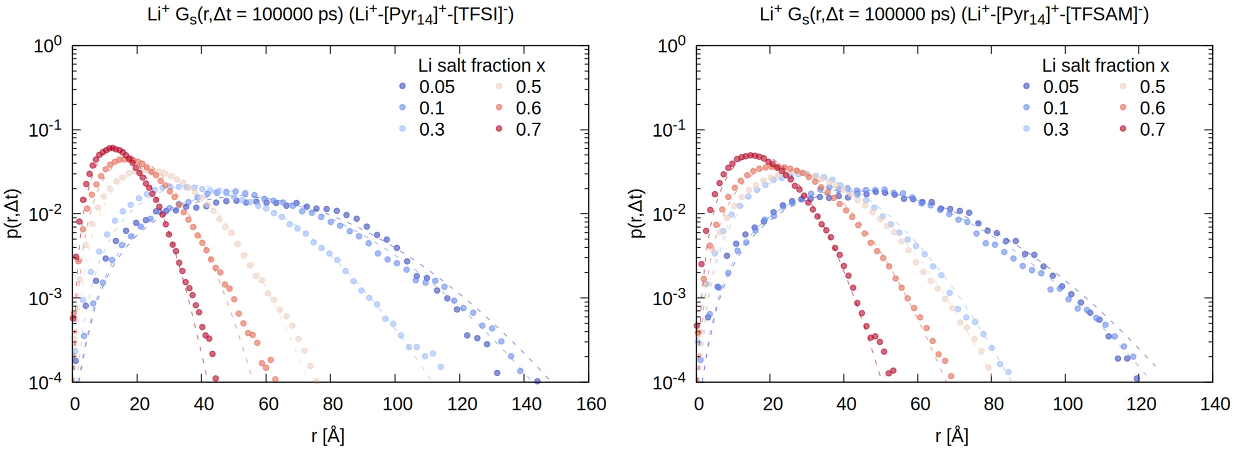

Figure S34: The self van Hove functions $G_s(r, \Delta t)$ of the lithium ions in TFSI$^-$ (left) and TFSAM$^-$ (right) containing electrolytes for the spectrum of investigated lithium salt concentrations x. $G_s(r, \Delta t)$ is compared to the corresponding ideal Gaussian distribution $G_{0,s}(r, \Delta t)$, which is depicted by the dashed lines.

P: Non-Gaussian parameter α_2

The non-Gaussian parameter (NGP) α_2 which probes the deviation from truly Gaussian dynamics, is extracted from the second and fourth moment of the particle displacements:

$$\alpha_2(t) = \frac{3}{5} \cdot \frac{\langle \Delta\vec{r}^{\,4}(t) \rangle}{\langle \Delta\vec{r}^{\,2}(t) \rangle^2} - 1, \tag{S16}$$

where $\Delta\vec{r}(t) = (\vec{r}(t) - \vec{r}(0))$ denotes the particle displacement within the time t and the brackets $< .. >$ indicate the ensemble average over all particles for the given time lag.

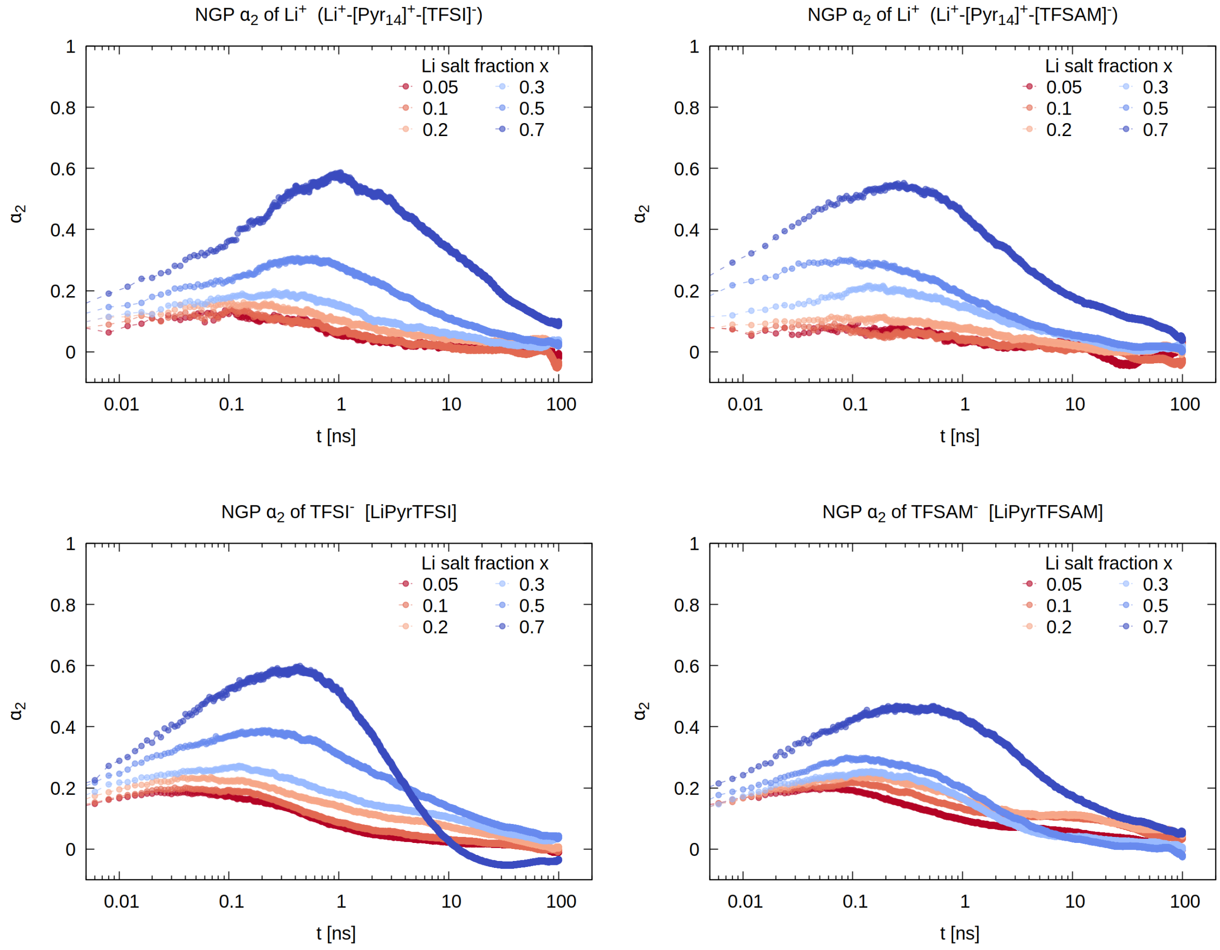

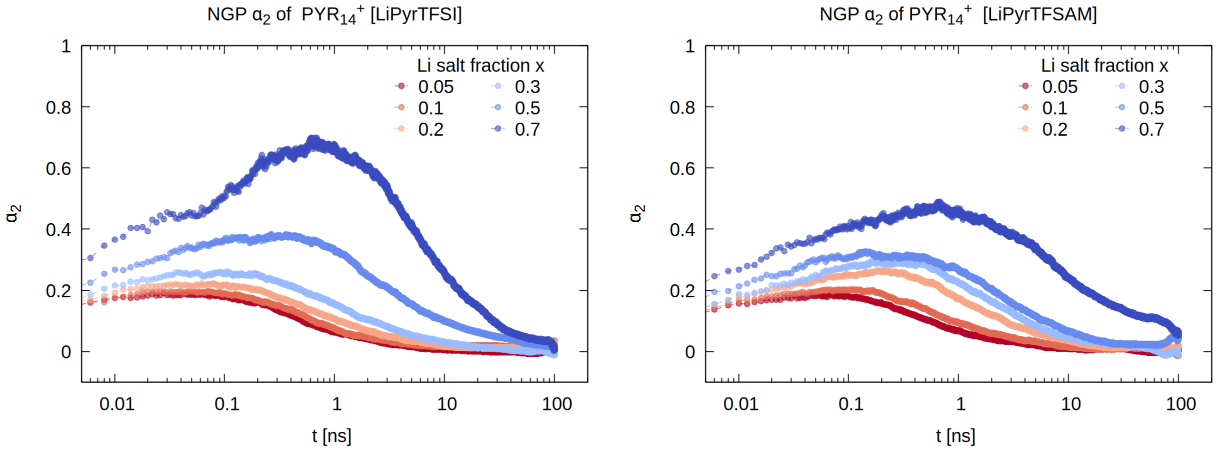

Figure S35: Non-gaussian parameters Li^+ (top), anions (middle) and Pyr_{14}^+ (bottom) dynamics in $TFSI^-$ (left) and $TFSAM^-$ (right) containing electrolytes for various lithium salt fractions x and averaging over 4 blocks of 100 ns duration each.

References

(1) Van Der Spoel, D.; Lindahl, E.; Hess, B.; Groenhof, G.; Mark, A. E.; Berendsen, H. J. GROMACS: Fast, flexible, and free. *Journal of Computational Chemistry* **2005**, *26*, 1701–1718.

(2) Páll, S.; Abraham, M. J.; Kutzner, C.; Hess, B.; Lindahl, E. Tackling Exascale Software Challenges in Molecular Dynamics Simulations with GROMACS. Solving Software Challenges for Exascale. Cham, 2015; pp 3–27.

(3) Abraham, M. J.; Murtola, T.; Schulz, R.; Páll, S.; Smith, J. C.; Hess, B.; Lindah, E. Gromacs: High performance molecular simulations through multi-level parallelism from laptops to supercomputers. *SoftwareX* **2015**, *1-2*, 19–25.

(4) Berendsen, H. J.; van der Spoel, D.; van Drunen, R. GROMACS: A message-passing parallel molecular dynamics implementation. *Computer Physics Communications* **1995**, *91*, 43–56.

(5) Jorgensen, W. L.; Maxwell, D. S.; Tirado-Rives, J. Development and testing of the OPLS all-atom force field on conformational energetics and properties of organic liquids. *Journal of the American Chemical Society* **1996**, *118*, 11225–11236.

(6) Gouveia, A. S.; Bernardes, C. E.; Tomé, L. C.; Lozinskaya, E. I.; Vygodskii, Y. S.; Shaplov, A. S.; Lopes, J. N. C.; Marrucho, I. M. Ionic liquids with anions based on fluorosulfonyl derivatives: from asymmetrical substitutions to a consistent force field model. *Physical Chemistry Chemical Physics* **2017**, *19*, 29617–29624.

(7) Canongia Lopes, J. N.; Pádua, A. A. CL&P: A generic and systematic force field for ionic liquids modeling. *Theoretical Chemistry Accounts* **2012**, *131*, 1–11.

(8) Canongia Lopes, J. N.; Deschamps, J.; Pádua, A. A. H. Modeling Ionic Liquids Using a Systematic All-Atom Force Field. *The Journal of Physical Chemistry B* **2004**, *108*, 2038–2047.

(9) Lopes, J. N.; Pádua, A. A. Molecular force field for ionic liquids composed of triflate or bistriflylimide anions. *Journal of Physical Chemistry B* **2004**, *108*, 16893–16898.

(10) Shimizu, K.; Almantariotis, D.; Costa Gomes, M. F.; Pádua, A. A.; Canongia Lopes, J. N. Molecular force field for ionic liquids V: Hydroxyethylimidazolium, dimethoxy-2methylimidazolium, and fluoroalkylimidazolium cations and Bis(fluorosulfonyl)amide, perfluoroalkanesulfonylamide, and fluoroalkylfluorophosphate anions. *Journal of Physical Chemistry B* **2010**, *114*, 3592–3600.

(11) Doherty, B.; Zhong, X.; Gathiaka, S.; Li, B.; Acevedo, O. Revisiting OPLS force field parameters for ionic liquid simulations. *Journal of chemical theory and computation* **2017**, *13*, 6131–6145.

(12) Bhargava, B. L.; Balasubramanian, S. Refined potential model for atomistic simulations of ionic liquid [bmim][PF6]. *The Journal of Chemical Physics* **2007**, *127*, 114510.

(13) Chaban, V. V.; Voroshylova, I. V.; Kalugin, O. N. A new force field model for the simulation of transport properties of imidazolium-based ionic liquids. *Physical Chemistry Chemical Physics* **2011**, *13*, 7910.

(14) Self, J.; Fong, K. D.; Persson, K. A. Transport in superconcentrated LiPF6 and LiBF4/propylene carbonate electrolytes. *ACS Energy Letters* **2019**, *4*, 2843–2849.

(15) Fong, K. D.; Self, J.; Diederichsen, K. M.; Wood, B. M.; McCloskey, B. D.; Persson, K. A. Ion transport and the true transference number in nonaqueous polyelectrolyte solutions for lithium ion batteries. *ACS central science* **2019**, *5*, 1250–1260.

(16) Molinari, N.; Mailoa, J. P.; Craig, N.; Christensen, J.; Kozinsky, B. Transport anomalies emerging from strong correlation in ionic liquid electrolytes. *Journal of Power Sources* **2019**, *428*, 27–36.

(17) Molinari, N.; Mailoa, J. P.; Kozinsky, B. General trend of a negative Li effective charge in ionic liquid electrolytes. *The journal of physical chemistry letters* **2019**, *10*, 2313–2319.

(18) Molinari, N.; Kozinsky, B. Chelation-Induced Reversal of Negative Cation Transference Number in Ionic Liquid Electrolytes. *The Journal of Physical Chemistry B* **2020**, *124*, 2676–2684.

(19) Huang, Q.; Lourenço, T. C.; Costa, L. T.; Zhang, Y.; Maginn, E. J.; Gurkan, B. Solvation Structure and Dynamics of Li+ in Ternary Ionic Liquid–Lithium Salt Electrolytes. *The Journal of Physical Chemistry B* **2018**, *123*, 516–527.

(20) Thum, A.; Heuer, A.; Shimizu, K.; Lopes, J. N. C. Solvate ionic liquids based on lithium bis (trifluoromethanesulfonyl) imide–glyme systems: coordination in MD simulations with scaled charges. *Physical Chemistry Chemical Physics* **2020**, *22*, 525–535.

(21) Lemkul, J. A.; Huang, J.; Roux, B.; MacKerell Jr, A. D. An empirical polarizable force field based on the classical drude oscillator model: development history and recent applications. *Chemical reviews* **2016**, *116*, 4983–5013.

(22) Salomon-Ferrer, R.; Case, D. A.; Walker, R. C. An overview of the Amber biomolecular simulation package. *Wiley Interdisciplinary Reviews: Computational Molecular Science* **2013**, *3*, 198–210.

(23) Li, Z.; Bouchal, R.; Mendez-Morales, T.; Rollet, A.-L.; Rizzi, C.; Le Vot, S.; Favier, F.; Rotenberg, B.; Borodin, O.; Fontaine, O. Transport Properties of Li-TFSI Water-in-Salt Electrolytes. *The Journal of Physical Chemistry B* **2019**, *123*, 10514–10521.

(24) Nürnberg, P.; Lozinskaya, E. I.; Shaplov, A. S.; Schönhoff, M. Li Coordination of a Novel Asymmetric Anion in Ionic Liquid-in-Li Salt Electrolytes. *The Journal of Physical Chemistry B* **2020**, *124*, 861–870.

(25) Martinez, L.; Andrade, R.; Birgin, E. G.; Martínez, J. M. PACKMOL: A package for building initial configurations for molecular dynamics simulations. *Journal of Computational Chemistry* **2009**, *30*, 2157–2164.

(26) Berendsen, H. J. C.; Postma, J. P. M.; van Gunsteren, W. F.; DiNola, A.; Haak, J. R. Molecular dynamics with coupling to an external bath. *The Journal of Chemical Physics* **1984**, *81*, 3684–3690.

(27) Bussi, G.; Donadio, D.; Parrinello, M. Canonical sampling through velocity rescaling. *The Journal of Chemical Physics* **2007**, *126*, 014101.

(28) Parrinello, M.; Rahman, A. Polymorphic transitions in single crystals: A new molecular dynamics method. *Journal of Applied Physics* **1981**, *52*, 7182–7190.

(29) Nosé, S.; Klein, M. Constant pressure molecular dynamics for molecular systems. *Molecular Physics* **1983**, *50*, 1055–1076.

(30) Nosé, S. A molecular dynamics method for simulations in the canonical ensemble. *Molecular Physics* **1984**, *52*, 255–268.

(31) Hoover, W. G. Canonical dynamics: Equilibrium phase-space distributions. *Physical Review A* **1985**, *31*, 1695–1697.

(32) Hess, B.; Bekker, H.; Berendsen, H. J. C.; Fraaije, J. G. E. M. LINCS: A linear constraint solver for molecular simulations. *Journal of Computational Chemistry* **1997**, *18*, 1463–1472.

(33) Hess, B. P LINCS:A Parallel Linear Constraint Solver for Molecular Simulation. **2007**,

(34) Michaud-Agrawal, N.; Denning, E. J.; Woolf, T. B.; Beckstein, O. MDAnalysis: a toolkit for the analysis of molecular dynamics simulations. *Journal of computational chemistry* **2011**, *32*, 2319–2327.

(35) Gowers, R. J.; Linke, M.; Barnoud, J.; Reddy, T. J. E.; Melo, M. N.; Seyler, S. L.; Domanski, J.; Dotson, D. L.; Buchoux, S.; Kenney, I. M. *MDAnalysis: a Python package for the rapid analysis of molecular dynamics simulations*; 2019.

(36) Li, Z.; Borodin, O.; Smith, G. D.; Bedrov, D. Effect of organic solvents on Li+ ion solvation and transport in ionic liquid electrolytes: a molecular dynamics simulation study. *The Journal of Physical Chemistry B* **2015**, *119*, 3085–3096.

(37) Haskins, J. B.; Bennett, W. R.; Wu, J. J.; Hernandez, D. M.; Borodin, O.; Monk, J. D.; Bauschlicher Jr, C. W.; Lawson, J. W. Computational and experimental investigation of Li-doped ionic liquid electrolytes:[pyr14][TFSI],[pyr13][FSI], and [EMIM][BF4]. *The Journal of Physical Chemistry B* **2014**, *118*, 11295–11309.

(38) Zhang, Z.; Nasrabadi, A. T.; Aryal, D.; Ganesan, V. Mechanisms of Ion Transport in Lithium Salt-Doped Polymeric Ionic Liquid Electrolytes. *Macromolecules* **2020**, *53*, 6995–7008.

(39) Williams, G.; Watts, D. C. Non-symmetrical dielectric relaxation behaviour arising from a simple empirical decay function. *Transactions of the Faraday society* **1970**, *66*, 80–85.

(40) Johnston, D. Stretched exponential relaxation arising from a continuous sum of exponential decays. *Physical Review B* **2006**, *74*, 184430.